Atmospheric Environment 133 (2016) 93–111

Contents lists available at ScienceDirect

Atmospheric Environment

journal homepage: www.elsevier.com/locate/atmosenv

NO and NOy in the upper troposphere: Nine years of CARIBIC measurements onboard a passenger aircraft

G. Stratmann [a, *], H. Ziereis [a], P. Stock [a], C.A.M. Brenninkmeijer [b], A. Zahn [c], A. Rauthe-Schöch [b], P.V. Velthoven [d], H. Schlager [a], A. Volz-Thomas [e, 1]

[a] Deutsches Zentrum für Luft- und Raumfahrt, Institut für Physik der Atmosphäre, Oberpfaffenhofen, Germany
[b] Max-Planck-Institut für Chemie (Otto-Hahn-Institut), Chemie der Atmosphäre, Mainz, Germany
[c] Karlsruhe Institut für Technologie, In-situ Measurements Onboard Aircraft, Karlsruhe, Germany
[d] Koninklijk Nederlands Meteorologisch Instituut, Chemistry and Climate Division, de Bilt, The Netherlands
[e] Forschungszentrum Julich, IEK-8, Jülich, Germany

HIGHLIGHTS

- Most comprehensive nitrogen oxide dataset available today for the upper troposphere.
- Longest NO and NO_y series of measurements over Europe in the upper troposphere.
- Clear seasonal cycles in NO and NO_y mixing ratios are found in defined region.
- NO_y boundary layer emissions are more important in the (sub)tropical regions.

ARTICLE INFO

Article history:
Received 20 July 2015
Received in revised form
20 February 2016
Accepted 23 February 2016
Available online 26 February 2016

Keywords:
Nitrogen oxide
Upper troposphere
Atmosphere
Airborne
Climatology
In-service aircraft

ABSTRACT

Nitrogen oxide (NO and NO_y) measurements were performed onboard an in-service aircraft within the framework of CARIBIC (Civil Aircraft for the Regular Investigation of the atmosphere Based on an Instrument Container). A total of 330 flights were completed from May 2005 through April 2013 between Frankfurt/Germany and destination airports in Canada, the USA, Brazil, Venezuela, Chile, Argentina, Colombia, South Africa, China, South Korea, Japan, India, Thailand, and the Philippines. Different regions show differing NO and NO_y mixing ratios. In the mid-latitudes, observed NO_y and NO generally shows clear seasonal cycles in the upper troposphere with a maximum in summer and a minimum in winter. Mean NO_y mixing ratios vary between 1.36 nmol/mol in summer and 0.27 nmol/mol in winter. Mean NO mixing ratios range between 0.05 nmol/mol and 0.22 nmol/mol. Regions south of 40°N show no consistent seasonal dependence. Based on CO observations, low, median and high CO air masses were defined. According to this classification, more data was obtained in high CO air masses in the regions south of 40°N compared to the midlatitudes. This indicates that boundary layer emissions are more important in these regions. In general, NO_y mixing ratios are highest when measured in high CO air masses. This dataset is one of the most comprehensive NO and NO_y dataset available today for the upper troposphere and is therefore highly suitable for the validation of atmosphere-chemistry-models.

1. Introduction

Ozone is one of the most important components of the short-lived greenhouse gases. Its concentration in the troposphere is controlled by transport from the stratosphere, by photochemical processes (destruction and production) involving, amongst other compounds, NO and NO_2 (=NO_x).

Nitrogen oxides play a dual role in the anthropogenic radiative forcing. Either they contribute to a positive radiative forcing by the

* Corresponding author. DLR-IPA, Münchenerstr. 20, 82234 Wessling, Germany.
E-mail addresses: Greta.Stratmann@dlr.de (G. Stratmann), Helmut.Ziereis@dlr.de (H. Ziereis), Paul.Stock@dlr.de (P. Stock), carl.brenninkmeijer@mpic.de (C.A.M. Brenninkmeijer), andreas.zahn@kit.edu (A. Zahn), armin.rauthe-schoech@mpic.de (A. Rauthe-Schöch), velthove@knmi.nl (P.V. Velthoven), Hans.Schlager@dlr.de (H. Schlager), a.volz-thomas@fz-juelich.de (A. Volz-Thomas).
[1] now at IAGOS-AISBL, Brussels, Belgium.

http://dx.doi.org/10.1016/j.atmosenv.2016.02.035

catalytic production of ozone or their contribution to the radiative forcing is negative due to their impact on the concentration of hydroxyl radicals and on the lifetime of methane (Fuglestvedt et al., 1999). Reduced methane concentrations imply reduced ozone production. In total the overall contribution of nitrogen oxides to the anthropogenic radiative forcing might even be negative (Stevenson et al., 2013). The ozone production efficiency strongly depends non-linearly on the background concentration of nitrogen oxides. The efficiency becomes greater with increasing nitrogen oxide concentrations, reaches a maximum (at a few hundred pmol/mol) and diminishes again with further increasing nitrogen oxide concentrations (Grooss et al., 1998; Liu et al., 1980). Therefore nitrogen oxide emissions in the upper troposphere and lower stratosphere (UTLS) (at lower background concentrations) lead to a higher ozone production efficiency there compared to the boundary layer where concentrations are generally higher (Dahlmann et al., 2011).

The radiative forcing of greenhouse gases depends, among other factors, on the difference between the temperature where the radiation is emitted and the temperature where it is absorbed. Therefore the radiative forcing is larger at the cold tropopause than elsewhere in the troposphere or stratosphere (e.g. Lacis et al., 1990).

Nitrogen oxides are usually emitted into the atmosphere as nitrogen monoxide (NO). Under daylight conditions a photostationary state between NO and NO_2 is established within a few minutes involving mainly oxidation by ozone and photolysis. Therefore the sum of these two nitrogen oxides is referred to as NO_x. Within hours to days, NO_x is oxidized into other reactive nitrogen compounds (Jaeglé et al., 1998; Bradshaw et al., 2000). NO_y is the sum of all reactive nitrogen species in the atmosphere. The most abundant species of this odd nitrogen family are, besides NO_x, nitric acid (HNO_3) and peroxyacetyl nitrate (PAN) (Bradshaw et al., 1999; Singh et al., 2007). Other common NO_y species are HONO, N_2O_5, HO_2NO_2, and NO_3. The main sink for nitric acid in the atmosphere is dry and wet deposition. Its lifetime in the UTLS depends on the convective turnaround of the atmosphere and therefore on region and season (Bertram et al., 2007). In warm conveyor belts and convective outflow nitric acid can be removed within one to three days (Miyazaki et al., 2003). In the dry UTLS, however, the lifetime can be in the order of weeks (Ehhalt et al., 1992). The lifetime of PAN against thermal decomposition and photolysis in the UTLS is of the order of several weeks (Talukdar et al., 1995). These long lifetimes allow the long-range transport of reactive nitrogen species at continental scales.

The concentration of reactive nitrogen species in the UTLS is controlled by a variety of processes and anthropogenic and natural sources, such as lightning, stratospheric input, air traffic emissions, soil microbiology, fossil fuel combustion, anthropogenic induced biomass burning, and wildfires (e.g. Grewe, 2007).

The combination of comparatively short lifetime, variety of sources, and complex chemistry entails large spatial variations in the levels of nitrogen oxides. Due to non-linear photochemistry, the ozone production efficiency also shows large spatial variations causing high uncertainty about the impact of nitrogen oxides on climate. Numerous field campaigns involving research aircraft have been performed over the years (Hegglin et al., 2006; Jaeglé et al., 1998; Ziereis et al., 2000). Attempts have been made to combine these different measurements into climatologies of nitrogen oxide measurements of the troposphere (Bradshaw et al., 2000; Emmons et al., 1997). However, dedicated aircraft campaigns are often biased, in the sense that they aim to study specific atmospheric issues, such as lightning, long-range transport, and aircraft emissions. As time and regional coverage are restricted, in particular trace constituents with a short lifetime and a variety of different sources, such as nitrogen oxide, are not represented adequately. To improve model simulations, a solid base of nitrogen oxide measurements is required (Holmes et al., 2011).

NO_y monitoring in the UTLS on a regular basis would help to improve the understanding of the chemistry in the UTLS. Routine observations from in-service aircraft can close the gap between individual measurement campaigns focused on specific questions, ground-based measurements, and satellite observations. In the long run they are suitable for providing a reliable basis for establishing a climatology. Measurements onboard commercial aircraft might be biased to a small extent due to flying along air traffic routes. Aircraft plumes from previous aircrafts are observed occasionally during CARIBIC flights. They are visible because of small scale (~2–40 s length) NO and NO_y peaks. In an extreme flight, small scale peaks occurred ~20 times during the flight. Even for this extreme flight the average NO_y mixing ratio is altered by only 3.3% due to crossing the fresh aircraft plumes (~3.5% of the flight duration). Usually much less or no peaks are detected during a flight. On average, fresh aircraft plumes account for only ~0.9% of the dataset. Therefore samplings of small scale NO and NO_y peaks caused by air traffic alter the average concentration only marginal.

Furthermore, commercial aircraft avoid flying through thunderstorms. Therefore very recent emissions from lightning are usually not encountered, but the encountered air masses itself are influenced by the outflow of thunderstorm clouds. A negative bias due to lightning is not expected. Large scale enhancements due to air traffic or lightning, two of the main NO_y sources, are included in this dataset.

Measurements of reactive nitrogen species onboard in-service aircraft go back to the early 1980s. Dickerson (1984) reported on the observation of NO, NO_2, and NO_y using a chemiluminescence detector system. The instrumentation was installed in an airfreight container onboard a German Cargo Boeing 707 aircraft. NO and NO_2 were also measured onboard in-service aircraft during the NOXAR (May 1995 through May 1996) and POLINAT-2 projects (August through November 1997). These measurements were performed on a Swissair B-747 during approx. 600 flights (Brunner et al., 2001; Jeker et al., 2000). For several years NO_y was measured regularly on one aircraft of the MOZAIC fleet, with the instruments installed permanently in the avionics bay of the in-service aircraft (Volz-Thomas et al., 2005).

A different approach is chosen by CARIBIC (**C**ivil **A**ircraft for the **R**egular **I**nvestigation of the Atmosphere **B**ased on an **I**nstrument **C**ontainer, http://www.caribic-atmospheric.com/). For CARIBIC an airfreight container with a payload of more than one ton is used to install a comprehensive set of in-situ instruments (CO, CO_2, NO, NO_y, O_3, CH_4, N_2O, organic compounds, mercury, water, aerosols, and more). During CARIBIC-1, an airfreight container was operated onboard a Boeing 767-300 of LTU International Airways between 1997 and 2002 (Brenninkmeijer et al., 1999). During CARIBIC-2, a modified container is installed in the cargo bay of a commercial airliner (Airbus A340-600 of Lufthansa) around once a month for four to six consecutive long-range flights (Brenninkmeijer et al., 2007). After test flights in December 2004, regular operation began in spring 2005. More than 370 flights have been made since then. The base of the CARIBIC deployment was Frankfurt airport (since summer 2014 Munich airport) in Germany. The main destinations are located in China, India, Venezuela, the USA, and Canada. Today, CARIBIC has been succeeded by IAGOS (IAGOS-CARIBIC; In-service Aircraft for a Global Observing System, www.iagos.org). The measurement of nitrogen oxides within CARIBIC is based on former experiences with the operation of similar sensors onboard research aircraft. Since the early 1990s chemiluminescence detectors have been used for observations in the free troposphere and lower stratosphere (e.g. Huntrieser et al., 2002; Schlager et al., 1997; Ziereis et al., 2004).

Over the last few years a comprehensive set of NO and NO_y data was obtained with the CARIBIC flying laboratory. Although the concentration of nitrogen oxides in the UTLS is highly variable, this dataset lays the foundation for a nitrogen oxide climatology in the upper troposphere, at least for the regions that are regularly covered by CARIBIC flights. The observations allow analysis of regional and seasonal differences in the concentrations.

2. Instrumentation

The CARIBIC airfreight container includes automated instruments for simultaneous measurements of atmospheric gases, aerosols, and trace compounds. A detailed description of the CARIBIC system is given in Brenninkmeijer et al. (2007). The NO and NO_y measurements within CARIBIC are performed using a two-channel chemiluminescence detector. Since the 1970s chemiluminescence (CL) techniques have been used for atmospheric nitrogen oxide measurements (Ridley and Howlett, 1974; Kley and McFarland, 1980; Schlager et al., 1997; Ziereis et al., 2000; Volz-Thomas et al., 2005). Light emissions from the reaction of NO with O_3 are detected using a cooled photomultiplier. A commercial two-channel chemiluminescence detector (SR 79501, ECO PHYSICS, Switzerland) is used for simultaneous measurements of NO and NO_y. NO_y is measured by a catalytic conversion technique using a gold tube (60 cm long, outer diameter 6.4 mm) maintained at 300°C and hydrogen as the reducing agent to convert the NO_y into NO. The resulting NO is detected using chemiluminescence. More detailed information on the NO_y catalytic conversion technique is given in Bollinger et al. (1983), Fahey et al. (1985) and Drummond et al., (1985).

Before the detector was installed in the CARIBIC container it was used during several airborne research campaigns (Schulte and Schlager, 1996; Feigl et al., 1999; Ziereis et al., 2000).

The CARIBIC inlet system is located near the belly fairing of the A340-600. It contains sample lines for trace gases and aerosols. The NO-NO_y sample lines are made of perfluoroalkoxy polymer (PFA) and are heated to ~ 40°C to avoid adsorption of highly polar NO_y species. The volume flow inside the sample lines is regulated by an orifice and is ~80–100 l/min. Because of this high volume flow and the heating of the inlet lines, only small memory effects of HNO_3 are expected. This is also confirmed by Neuman et al. (1999). The residence time inside the sample lines is approx. 0.8 s under typical measurement conditions. Inside the NO-NO_y instrument a constant sample air-mass flow of 1.6 l/min is established for the two detectors by needle valves in combination with a critical orifice in the detector inlet lines. The measuring system is calibrated before and after each flight period in the laboratory by multipoint calibration. The conversion efficiency of the gold converter is quantified using gas phase titration of NO and O_3 before and after each flight. The conversion efficiency was 98% on average between 2005 and 2013. The average sensitivity is 15 counts per second (cps)/(pmol/mol) for the NO measurements, and 14 cps/(pmol/mol) for the NO_y measurements, respectively. The variation of the sensitivity before and after four consecutive flights is approx. 4%. Every 4 h during a flight, synthetic air is added to the sample lines in order to determine the instrument offset. The offset is approx. 8 pmol/mol (±27%) on average for the NO measurements, and 120 pmol/mol (±10%) on average for NO_y measurements.

The statistical detection limit is 7 pmol/mol for the NO measurements and 8 pmol/mol for the NOy measurements for an integration time of 1 s. The overall uncertainty for the NO and NO_y measurements is 8% (6.5%) for volume mixing ratios of 0.5 nmol/mol (1 nmol/mol). Interferences of other NO_y constituents are not considered. However, an additional uncertainty arises from the conversion of HCN. We studied the HCN conversion by applying a known amount of HCN to the instrument. As the conversion might depend on ozone, we changed the ozone concentrations (0–96 nmol/mol). While Volz-Thomas et al. (2005) found a conversion efficiency of about 100%, our measurements showed a much lower conversion of about 3–18%, depending on the O_3 concentration. The global upper tropospheric HCN concentration is about up to 0.2 nmol/mol (Li et al., 2003). Thus, the HCN interference amounts to approx. 6–36 pmol/mol.

In this study CO and O_3 data and trajectory calculations obtained within CARIBIC are used for analysis. CO measurements are performed using vacuum ultraviolet resonance fluorescence (Scharffe et al., 2012; Gerbig et al., 1996). The instrument is operated with a time resolution of 1s and in-flight calibration every 25 min. The precision of the measurement is 1.6 nmol/mol for high resolution data (1 s) and 1 nmol/mol for 10 s averages. O_3 is measured using a combination of a UV photometer and a dry chemiluminescence detector (Zahn et al., 2012). 5-day backward trajectories are calculated every 3 min along the flight track using the KNMI TRAJKS trajectory model (Scheele et al., 1996) and meteorological analyses from the European Centre for Medium-Range Weather Forecasts (ECMWF). More details can be found in the referenced literature.

3. Overview of the measurements

The CARIBIC flying laboratory is installed around once a month on two to six consecutive flights onboard a specific Lufthansa A340-600. The missions either consist of a long-range flight in combination with a short-range one and then back to Frankfurt (e.g. Frankfurt-Guangzhou-Manila-Guangzhou-Frankfurt) or of the combination of two return flights from Frankfurt. The mean flight duration is around 9 h. The flight paths are located between 124°W and 142°E and between 78°N and 35°S (see Fig. 1). The CARIBIC measurements mostly take place at cruise-level altitudes in the UTLS, at heights up to 180 hPa.

For the analyses in this study, all NO and NO_y data obtained through April 2013 have been used. In total, nitrogen oxide data was obtained from around 74% of all CARIBIC flights. Missing data was caused by accidental container switch-off or by instrument failure. Around 1310 h of NO_y data and 610 h of NO data were sampled. The lower amount of NO data is due to the fact that at night all NO is converted into NO_2. Therefore NO measurements are below the detection limit. These data is excluded from the data set. Around 54% of all CARIBIC flights were made at night, depending on the flight route and season. NO and NO_y measurements were only performed for atmospheric pressures lower than 500 hPa, i.e. at altitudes higher than approx. 5 km. Additionally, NO_x was calculated for the dataset using measured NO and O_3 and assuming a photostationary steady state. The photolysis rate was calculated using the Tropospheric Ultraviolet and Visible (TUV) Radiation Model v4.1 (Madronich et al., 2002). The model can be used at http://cprm.acd.ucar.edu/Models/TUV/Interactive_TUV/. Since O_3 measurements are not available for every NO measurement, NO_x cannot be calculated for the entire NO dataset. Because deviations from the equilibrium are not considered, calculated NO_x is only a first order approximation.

The Airbus A340-600 that is used as the carrier for the CARIBIC container is a long-haul aircraft mainly used by Lufthansa for flights to intercontinental destinations. Its flight schedule is adjusted by Lufthansa twice a year. The CARIBIC team has no say in which destinations are selected by Lufthansa but can choose on which flights, i.e. to which destinations, the CARIBIC container will be onboard the aircraft. During the CARIBIC-2 period the main destinations have been Guangzhou/China, Caracas/Venezuela, Chennai/India, Vancouver/Canada and São Paulo/Brazil. In 2005 most of the CARIBIC flights were performed between Frankfurt and São Paulo

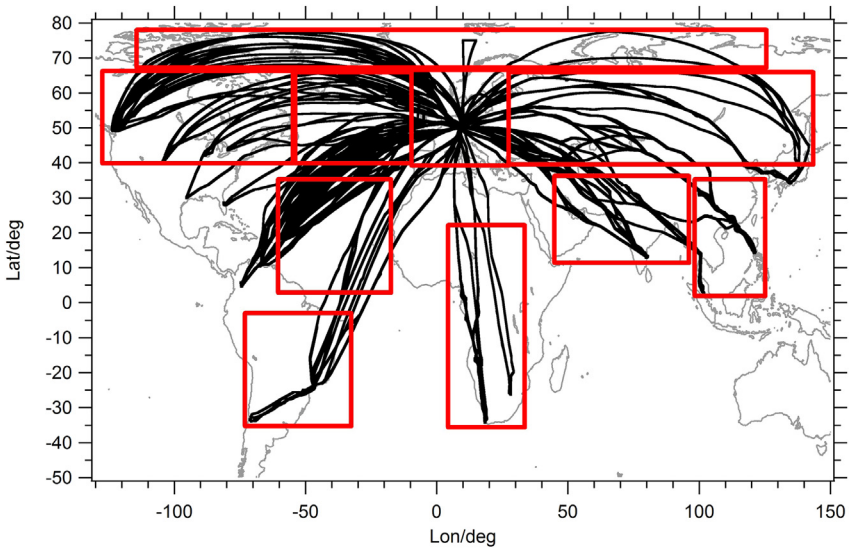

Fig. 1. CARIBIC flight routes (black) between May 2005 and April 2013 and the ten defined regions (gray): Arctic, North America, North Atlantic, Europe, North Asia, Sub/Tropical Atlantic, South America, Africa, North Asia, South Asia W, and South Asia E.

and Santiago de Chile/Chile. In 2006 and 2007 the main destinations were Guangzhou/China and Manila/the Philippines, in 2008 Chennai/India, and in the following years Caracas/Venezuela and Vancouver/Canada. Only 13 flights were made to destinations in South Africa. Approx. 93% of all data was obtained in the northern hemisphere. Details of the flight destinations can be found on the CARIBIC website.

3.1. Nitrogen oxide sources and their distribution

Nitrogen oxides from surface sources can be lofted from the boundary layer by convection or conveyor belts linked to weather fronts and then undergo long-range transport in the free troposphere. Anthropogenic sources (e.g. combustion of fossil fuels) are basically located in the northern hemisphere, e.g. the European Union, the USA, and newly industrializing countries in Southeast Asia. While anthropogenic NO_x emissions are declining or show stable concentrations in industrial countries (urban sites in the USA, e.g. (Russell et al., 2012); Germany, e.g. (Kurtenbach et al., 2012)) due to technological improvements and mitigation strategies, emissions in newly industrializing countries are increasing (e.g. in China, see (Zhang et al., 2007)).

Emission rates are typically expressed in Tg N per annum. The majority of N with approx. 28.5 Tg/a is emitted by combustion processes (fossil fuels and biomass) in the boundary layer (Schumann and Huntrieser, 2007). Soil microbiology has been estimated to contribute approx. 5.5 Tg/a, lightning 5.0 Tg/a, air traffic emissions 0.7 Tg/a, and N_2O degradation in the stratosphere 0.4 Tg/a to the atmospheric N budget (Schumann and Huntrieser, 2007).

To take into account regional differences in sources, sinks and distribution of atmospheric nitrogen oxides, the data was separated into ten different regions (Fig. 1 and Table 1): North America, South America, North Atlantic, Sub/Tropical Atlantic, Europe, North Asia, South Asia E, South Asia W, Africa, and the Arctic.

Seasonal and regional differences in the distribution of nitrogen oxides result from the specific source characteristic and the prevailing transport patterns. Turbulent mixing and transport mechanisms like convective transport are strongest in the summer months due to the heating of the Earth's surface. Also, lightning occurs more frequently in the summer months. Seasonal cycles in fossil fuel burning can be observed in the CO_2 seasonal cycle (Rotty, 1987). Fossil fuel burning in the boundary layer shows a slight maximum in the northern hemisphere in January due to domestic heating. Biomass burning is in large part anthropogenically induced and occurs all over the world in every season (Dwyer et al., 2000; Duncan et al., 2003). However, it peaks in the dry seasons in the tropics and in summer elsewhere. Biomass burning plumes have already been detected several times by CARIBIC (Lai et al., 2010; Ebinghaus et al., 2007), e.g. in Southeast Asia and on the west coast of South America. Air traffic occurs in large parts of the northern hemisphere in every season. A slight seasonal cycle exists, peaking in the late summer months (Eyers et al., 2005).

Table 1
Classifications of the different regions.

	Region	Longitude	Latitude
mid-latitudes	North America	125°W–55°W	66°N–40°N
	North Atlantic	53°W–12°W	66°N–40°N
	Europe	28°W–12°E	66°N–40°N
	North Asia	30°E–142°E	66°N–40°N
other	South Asia W	45°E–99°E	35°N–10°N
	South Asia E	99°E–125°E	35°N–0°N
	Africa	0°E–35°E	20°N–35°S
	Tropical Atlantic	60°W–12°W	30°N–5°S
	South America	75°W–28°W	3°S–35°S
	Arctic	160°W–160°E	90°N–66°N

Besides aviation, lightning is a local source of nitrogen oxide in the UTLS. Recent aircraft observations narrowed the uncertainty range of the global production rate of nitrogen oxides by lightning. NO_x production from lightning was estimated at 3–5 Tg N yr^{-1} (Schumann and Huntrieser, 2007). Based on satellite observations, Miyazaki et al. (2014) estimated the global source strength of lightning NO_x at approx. 6.3 ± 1.4 Tg N yr^{-1}.

Besides local sources and rapid transport of ground emissions within convective cells, the budget in the UT is also controlled by long-range transport (Cooper et al., 2010). Several studies have addressed long-range transport in connection with warm conveyor belts. Huntrieser et al. (2005), for example, observed a number of polluted layers of North American origin in the free troposphere

over Europe.

3.2. Discriminating between tropospheric and stratospheric air masses

Nitrogen oxides in the stratosphere and troposphere are controlled by different sources. While in the troposphere a variety of natural and anthropogenic sources control the NO_y budget, the main source in the stratosphere is the photooxidation of N_2O, mainly in the upper tropical stratosphere. For a better comparison with other datasets this paper focusses on the data obtained in the troposphere. Stratospheric data will be discussed in a separate publication.

The dynamical tropopause definition is used to discriminate between data obtained in the UT and in the LS. The potential vorticity (PV) is often used as a criterion for the tropopause (e.g. McCormack and Hood, 1997; Slemr et al., 2009; Roiger et al., 2011). The PV increases rapidly above the tropopause due to the increasing stability of the atmosphere. PV is indicated in potential vorticity units (1 PVU = 10^6 m^2 s^1 K kg^1). Here we use the potential vorticity value of 2 PVU from ECMWF meteorological data for the discrimination between tropospheric and stratospheric data. This value was first suggested by Hoskins et al. (1985). The PV definition fails near the equator, because here the Coriolis parameter, which is needed for the calculation of the absolute vorticity, is not defined. Therefore in the tropics the potential vorticity cannot be used as a criterion to divide our dataset into a stratospheric and tropospheric subset, respectively. However, in the tropics the tropopause altitude is always located above the flight altitude of the CARIBIC aircraft. Stratospheric influenced data might not be excluded completely by using the PV as the criterion. However, the effect on the overall tropospheric mean mixing ratios is negligible. Altogether, 14% (6%) of the NO_y (NO) data is measured in the tropics (20°S–20°N), and 86% (94%) in the extratropics. Here, around 47% (44%) of the data is measured in the troposphere. 0.3% of the tropospheric NO_y data is measured between 5 and 8 km, 11.7% between 8 and 10 km, 85.8% between 10 and 12 km and 2.2% between 12 and 14 km.

4. Results and discussion

4.1. Seasonal distribution of NO and NO_y mixing ratios at mid-latitudes (66°N – 40°N): Europe, North Asia, North America, North Atlantic

Around 30% of the tropospheric CARIBIC NO and NO_y data was obtained at northern mid-latitudes (40°N – 66°N). For further analyses the data obtained at mid-latitudes has been divided into four different regions: North America, North Atlantic, Europe, and North Asia (see Table 1).

4.1.1. Europe (12°W–28°E, 66°N–40°N)

Because Frankfurt in Germany was the base of the CARIBIC observations, a large percentage of the data was obtained during flights out of and on the way to this airport over Europe. The Europe box therefore shows the highest coverage of data of all regional boxes allowing a reliable statistical analysis. Fig. 2 shows NO, NO_y, NO_x, and CO volume mixing ratios obtained over the different regions. Although Fig. 2 starts with North America (first the mid-latitudes from west to east are shown), we start the discussion with Europe, since it is in this region that the highest data coverage was obtained. Fig. 2 (c) shows NO, NO_y, NO_x, and CO volume mixing ratios obtained over Europe. The data was averaged over a period of one month. NO_y shows a distinct seasonal cycle with a maximum in July (~1.3 nmol/mol) and a minimum in January (~0.3 nmol/mol). A similar seasonal behavior was also observed for NO with a maximum in July (0.3 nmol/mol) and a minimum in February (~0.1 nmol/mol). Enhanced NO mixing ratios are also observed in November; however, this monthly mean value comprises only 195 10 s mean values (average monthly 10 s mean values without November: ~1200). Additionally, Fig. 2 (c) shows the calculated NO_x seasonal cycle. In the upper troposphere, NO_x mainly consists of NO due to the temperature dependent reaction of NO with O_3 and increasing NO_2 photolysis (Ehhalt et al., 1992; Ziereis et al., 2000). Because calculated NO_x is only a first order approximation it is not discussed.

In recent years nitrogen oxides have been observed during several other aircraft missions in the tropopause region over Europe (Fiedler et al., 2009; Voigt et al., 2010; Hegglin et al., 2006). Although those studies were devoted to specific scientific issues, such as intercontinental transport, the climate impact of contrails, and trace gas transport in the tropopause region, their results can be used to compare with CARIBIC measurements, keeping in mind their smaller representativeness for average conditions.

During INTEX-B in May 2005, Fiedler et al. (2009) measured, amongst other trace gases, NO_y in an East Asian pollution plume over Europe. Inside the plume they found approx. 0.6 nmol/mol NO_y, and outside the plume they found 0.3 nmol/mol NO_y. In November 2001 during CONTRACE a number of polluted layers of North American origin were observed by Huntrieser et al. (2005) over Europe. They measured ~0.05 nmol/mol NO, 0.5–1.1 nmol/mol NO_y in the layer, and 0.1–0.3 nmol/mol background NO_y. In October/November 2008 during CONCERT, Voigt et al. (2010) measured 0.05–0.1 nmol/mol NO inside and approx. < 0.05 nmol/mol NO outside contrails over Europe. In general the results of these measurements fall within the range of the CARIBIC dataset (see Fig. 2 (c)).

The ratio between NO and NO_y can provide rough information about the age of the air mass (Wang et al., 2000). NO_y is primarily injected into the atmosphere from primary sources as NO. Oxidation processes involving OH and peroxy radicals transform NO into more long-lived NO_y species (e.g. HNO_3, PAN). The NO/NO_y ratio observed within CARIBIC over Europe ranges between 0.05 and 0.3 (not shown). A low ratio indicates that the air mass already underwent chemical processing (Jaeglé et al., 1998). A freshly polluted air mass therefore has a higher ratio than a chemical-aged air mass. The NO/NOy ratio does not show a distinct seasonal cycle, therefore it is not shown in Fig. 2.

To identify the specific source of the observed nitrogen oxides, we also use CO data, which is measured simultaneously. The long-lived (around 2 months (Edwards et al., 2004)) CO is a tracer for anthropogenic pollution from the boundary layer. It is a product of incomplete combustion processes. The main source is fossil fuel and biomass burning (e.g. Pétron et al., 2004). Biomass burning includes forest fires as well as savannah fires, biofuel burning, and garbage incineration. The NO_y/CO ratio depends on the background concentrations of NO_y and CO, the emission ratio, the loss and ageing process of the air mass, and the dilution with ambient air (Parrish et al., 1991; Eckhardt et al., 2003; Stohl et al., 2002). For example, a typical NO_y/CO ratio for biomass burning ranges between 0.008 and 0.1 (Buhr et al., 1995, quoted in Stohl et al., 2002). Biomass burning plumes were detected several times with CARIBIC, e.g. in October 2005 during two flights between São Paulo/Brazil and Santiago de Chile/Chile and in October 2006 during a flight from Guangzhou/China to Frankfurt/Germany (not shown). If the section of the flights with the biomass burning signature is extracted, its NO_y/CO molar mixing ratio is ~0.007, ~0.006, and ~0.01, which is in accordance with Buhr et al. (1995). The CO seasonal cycle in the UT over Europe (see Fig. 2 (c)) has its maximum (~120 nmol/mol) in spring and its minimum (~80 nmol/mol) in

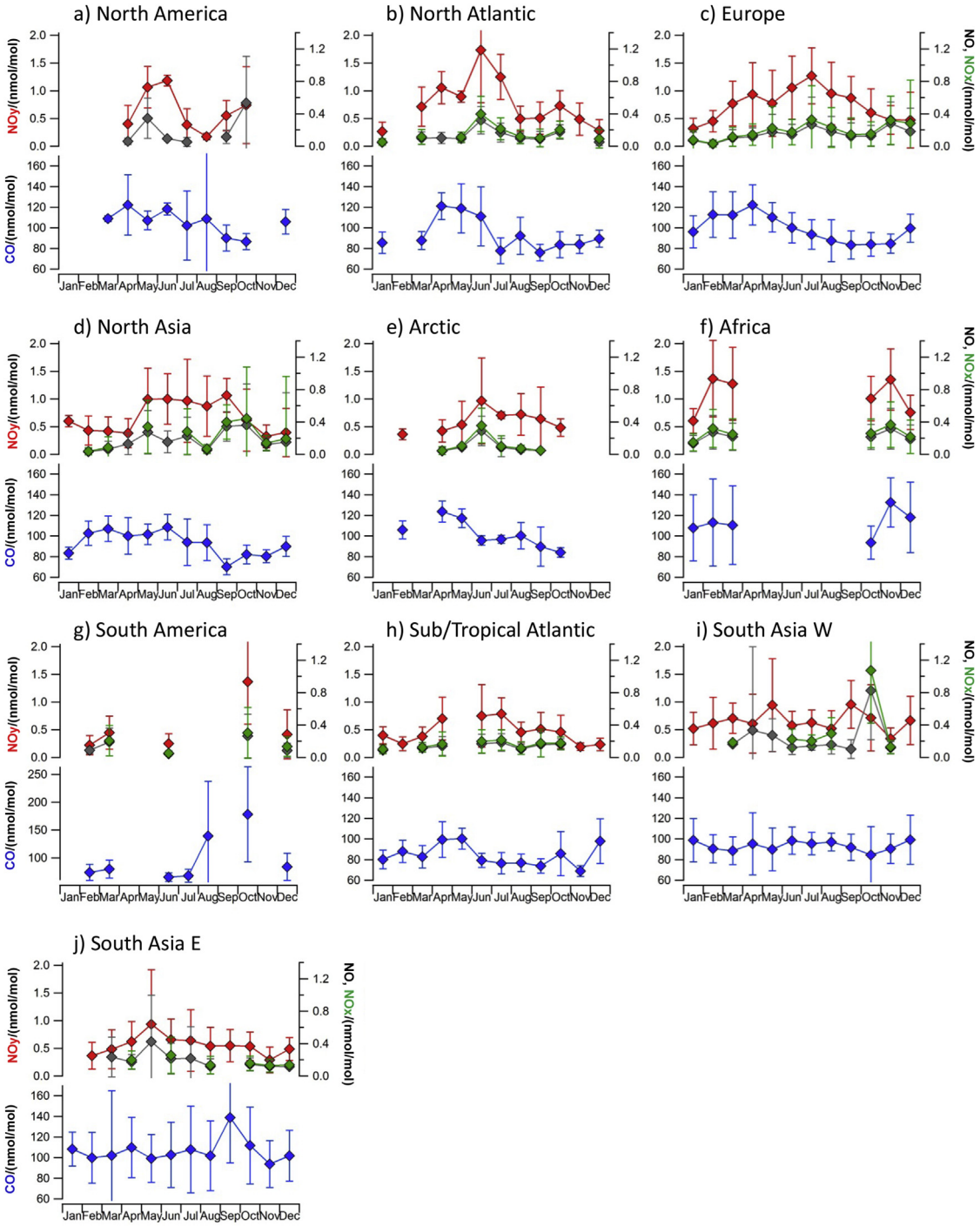

Fig. 2. Seasonal cycles of observed NO_y (black circles), NO (gray squares), CO (black squares, lower panel), and calculated NO_x (black squares, upper panel) between 2005 and 2013 in different regions. Data points have been averaged over one month. The bars denote the standard deviation.

autumn. The CO seasonal cycle results from the OH seasonal cycle and from the strength of the anthropogenic CO sources. Zahn et al. (2002) already analyzed CO measured within CARIBIC-1 in the northern hemispheric upper troposphere. They obtained comparable results. A positive correlation would indicate that NO_y and CO originate from the same anthropogenic boundary layer sources. Fig. 3 shows the scatter plot between tropospheric NO_y and CO for every season in all regions. Fig. 3 (c) shows the scatter plot between tropospheric NO_y and CO in Europe. CO ranges between approx. 60–150 nmol/mol and NO_y between approx. 0.01–3.5 nmol/mol. No explicit correlation is visible. To identify NO_y-CO correlations as mentioned above, single flights must be analyzed separately. Here, we want to give an overview of the total air masses in a regional box.

To get a better idea of the bulk of the NO_y data, the median NO_y volume mixing ratio for each season is also shown in Fig. 3.

As the measurements were not biased by specific research questions, the median CO value is considered as the background concentration. We define three different CO regimes: low (CO < median CO − 15%), median (median CO ± 15%), and high

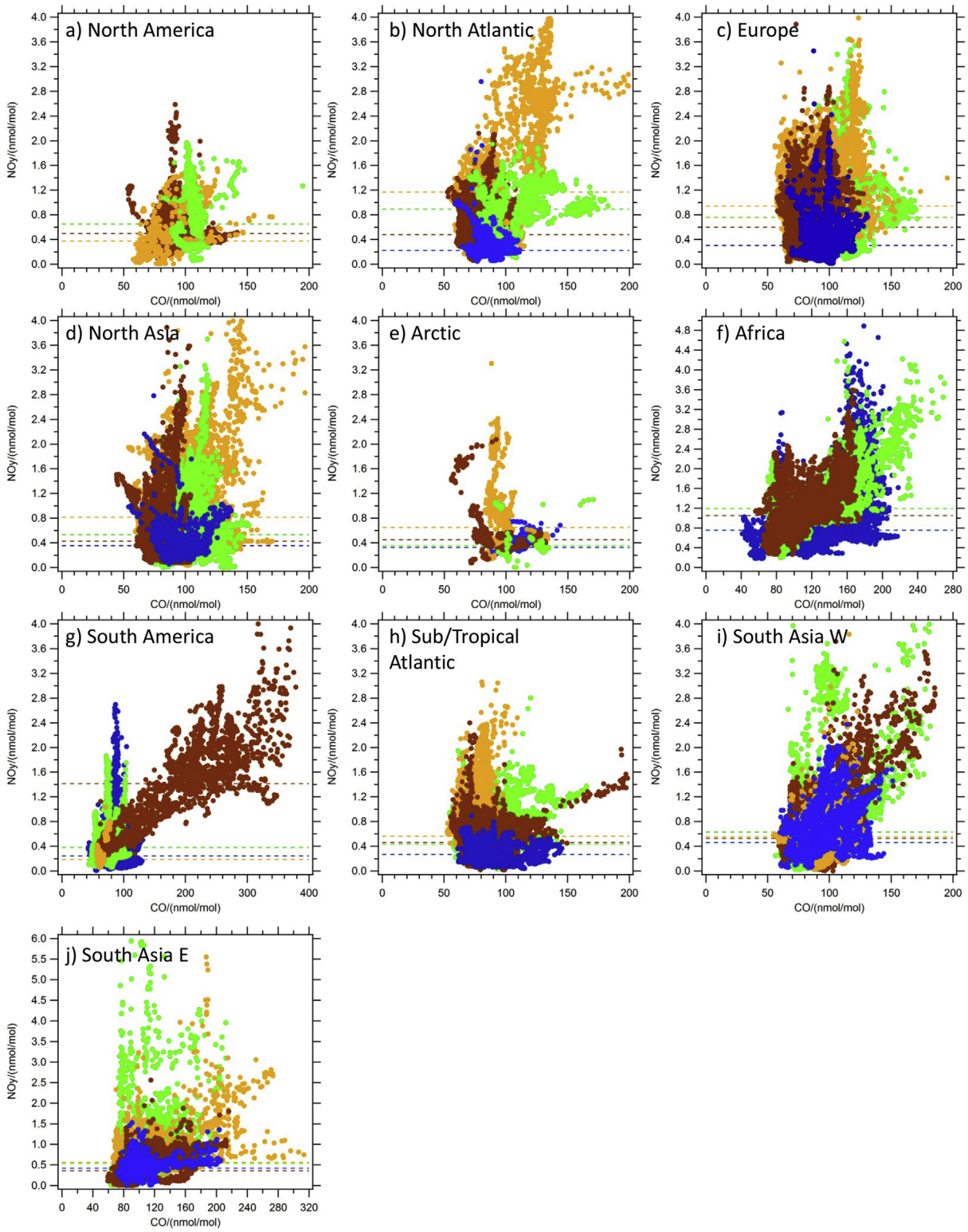

Fig. 3. NO_y versus CO volume mixing ratios for all seasons (green: MAM, orange: JJA, brown: SON, blue: DJF) obtained in the different regions between 2005 and 2013. Median NO_y volume mixing ratios for each season are indicated by horizontal lines. For North America no measurements were performed in DJF. Note the changed x-axis in South Asia E (up to 320 nmol/mol), South America (up to 400 nmol/mol), and Africa (up to 280 nmol/mol). Note the changed y-axis in South Asia E (up to 6 nmol/mol) and Africa (up to 5 nmol/mol).

(CO > median CO + 15%) CO air masses. Fig. 4 shows the fraction of NO_y measured in high CO air masses for the different regions. Median CO is shown in Table 2. According to the above-mentioned classification, Fig. 4 (a) (Europe, dark blue) shows that ~ 3–18% of the data was detected in high CO air. Mixing ratios observed in median or low CO air masses indicate that lightning, clean industrial combustion processes like electricity generating plants (Duncan et al., 2007), or aircraft may be the contributing sources

(Jaeglé et al., 1998). Certainly, measured NO_y originates from a mixture of different sources. Fig. 5 shows the NO_y mixing ratio in low, median, and high CO air masses (as defined above) in all seasons in every region. The mixing ratio in Europe is highest in high CO air masses. If the air mass originates from the boundary layer, the mean NO_y mixing ratio is higher than in median or low CO air.

The almost continuous NO and NO_y time series obtained over Europe allows the study of the annual cycle of nitrogen oxides for the whole sampling period (Fig. 6).

One month contains on average 4280 NO_y and 3210 NO 10 s mean data points. Maximum NO_y in summer and minimum NO_y in winter can be found for every year. The same is true for NO.

The variability within the time series is high, which obscures a possible trend. Satellite NO_2 measurements show that, due to the implementation of technological improvements (e.g. catalytic converters on automobile exhaust systems), a decreasing trend is observed over Europe and the central east coast of the United States (Richter et al., 2005). The satellite instrument retrieves tropospheric columns of NO_2, thus the columns observed from space are dominated by NO_2 in the boundary layer (Richter et al., 2005).

The present CARIBIC dataset provides the first long-term time series of NO and NO_y measurements in the upper troposphere. Long-term observations of NO_y have been performed at ground stations such as at the Jungfraujoch in the scope of the Global Atmosphere Watch (GAW) program (Pandey Deolal et al., 2012). However, no other long-term observational dataset of nitrogen oxides in the UT has existed until now.

4.1.2. North Asia (30°E–142°E, 66°N–40°N)

Fig. 2 (d) presents the seasonal cycle of NO, NO_y, NO_x, and CO measurements over North Asia. The data was obtained during flights between Frankfurt and Seoul/South Korea, Osaka/Japan, Guangzhou/China, Bangkok/Thailand, and Chennai/India. This region shows a clear seasonal NO_y cycle with a broad maximum between May and September (~1.0 nmol/mol) and a minimum in November (~0.3 nmol/mol). The NO seasonal cycle shows a minimum in winter and early spring (~0.05–0.15 nmol/mol) and a maximum in September/October (~0.35 nmol/mol). NO/NO_y ranges between 0.08 in February and 0.35 in November (not shown).

Fig. 3 (d) shows the scatter plot between NO_y and CO in North Asia. The values range roughly between ~60 and 160 nmol/mol for CO and between ~0.01 and 4.0 nmol/mol for NO_y. Enhanced NO_y mixing ratios up to around 4.0 nmol/mol were detected along with CO mixing ratios from 80 to 140 nmol/mol. There is no clear correlation between NO_y and CO. This shows a mixing between different air masses, with no clear signature of a single source.

As described above, low, median and high CO air masses are defined (see Table 2). On an annual average ~18% of NO_y was detected in high CO air (see Fig. 4 a, purple). Compared to Europe, in North Asia 8% more NO_y was measured in high CO air. This indicates that in North Asia lofted polluted air masses from the boundary layer are on an annual average a stronger NO_y source than in Europe (18% vs. 10%). Fig. 5 shows the NO_y mixing ratio in low, median, and high CO air masses in all seasons.

Table 2
Median CO mixing ratios (nmol/mol) in the different regions in all seasons, used for the definition of low, median, and high CO air masses. Median CO mixing ratios ±15% are defined as median CO air, smaller ratios are defined as low CO air, and larger ratios are defined as high CO air.

Season	Region	Median	Region	Median
MAM	North	108.1	South	80
JJA	America	97.4	America	72.6
SON		88.2		183.8
DJF		104.9		79.0
MAM	North	105.8	Tropical	89.6
JJA	Atlantic	89.7	Atlantic	76.1
SON		76.9		75.9
DJF		87.5		86.5
MAM	Europe	113.1	Africa	97.1
JJA		90.9		–
SON		81.8		101.8
DJF		100.4		106.2
MAM	Artic	118.6	South	86.6
JJA		97.1	Asia W	96.8
SON		84.9		89.4
DJF		107.3		93.1
MAM	North	102.0	South	91.9
JJA	Asia	94.6	Asia E	91.1
SON		81.0		94.5
DJF		95.1		95.4

4.1.3. North America (125°W–55°W, 66°N–40°N)

Fig. 2 (a) shows the seasonal NO_y, NO, and CO cycles for North America. This dataset was obtained along the flight tracks between Frankfurt and Vancouver/Canada, Toronto/Canada, Denver/USA, Chicago/USA, and Houston/USA. NO_y shows a seasonal cycle with a maximum in June (~1.19 nmol/mol) and a minimum in August (~0.39 nmol/mol). Note that no data was obtained between November and March. The NO seasonal cycle roughly follows the NO_y seasonal cycle, but with its maximum in October (~0.53 nmol/mol) and its minimum in July (~0.05 nmol/mol). In contrast to the seasonal NO and NO_y cycles in Europe and North Asia, the mixing ratios decrease sharply after the maximum.

Several measurement campaigns were already conducted over the United States. Previous studies by Brunner et al. (2001) and Cooper et al. (2009) showed that in spring/summer elevated NO and NO_y mixing ratios dominate in the UT region in the South East USA. They explain these values by high lightning activity over the south east coast of the USA. However, these previous observations of nitrogen oxides over the United States are not comparable to the CARIBIC measurements, because here the majority of the data was obtained north of 50°N and west of approx. 80°W. Nevertheless,

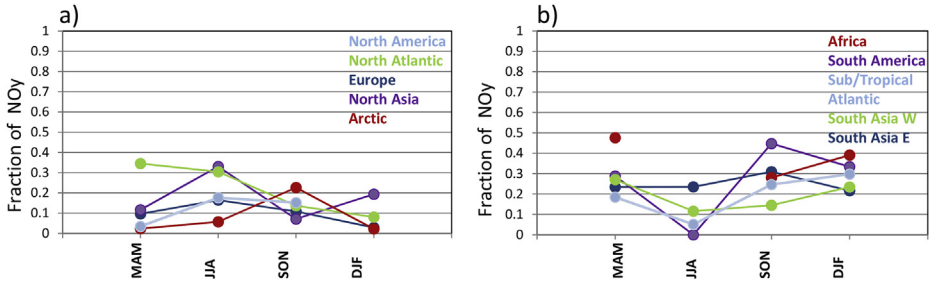

Fig. 4. Fraction of NO_y measured in high CO air masses in the northern (>40°N, a) and southern (<40°N, b) regions. See text for more information.

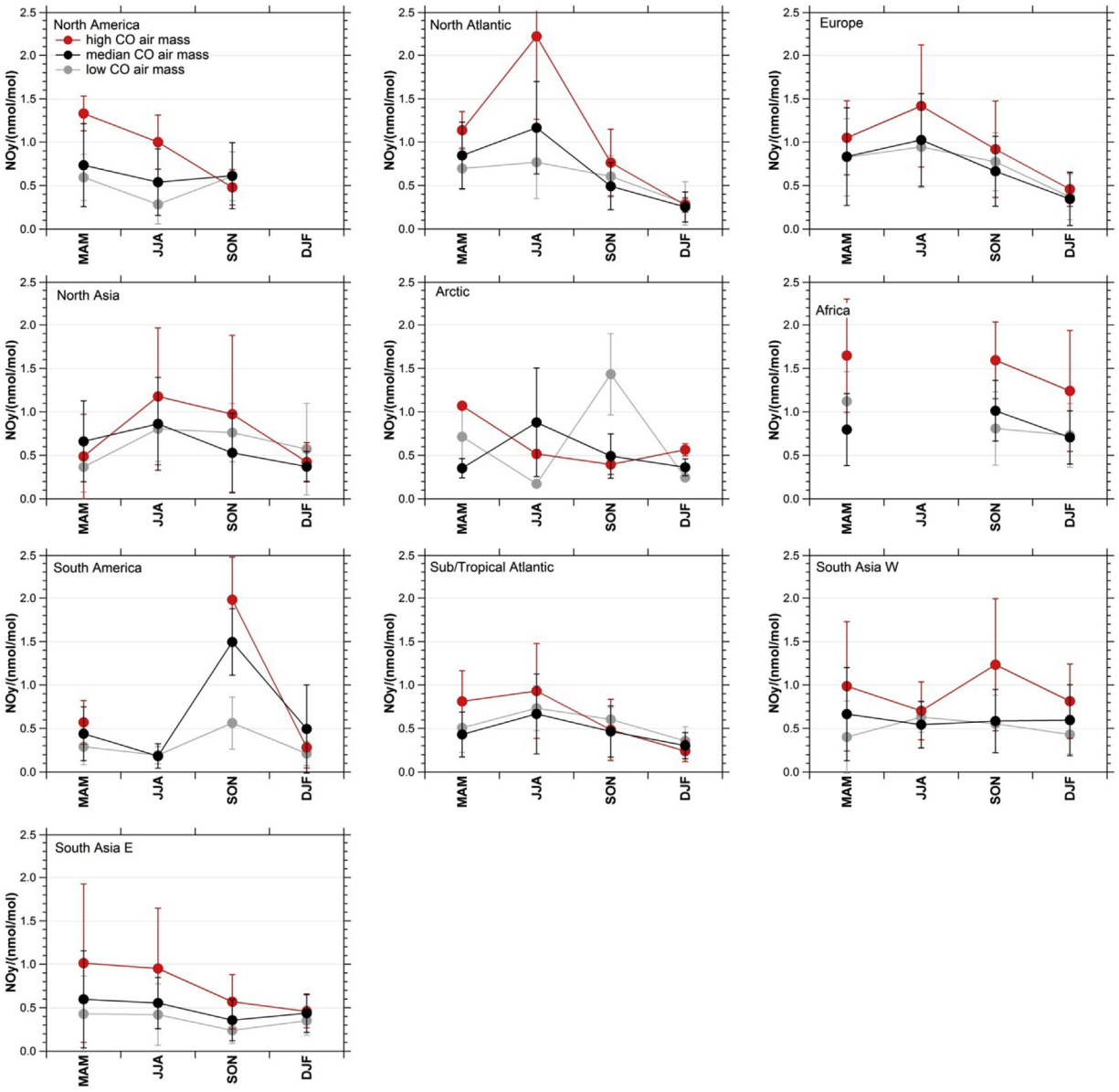

Fig. 5. Mean NO_y mixing ratios measured in low (gray line), in median (black line), and in high (dashed line) CO air masses (see text for more information) in every region and season. The bars denote the standard deviation. Mixing ratios are only shown if more than 30 data points are available.

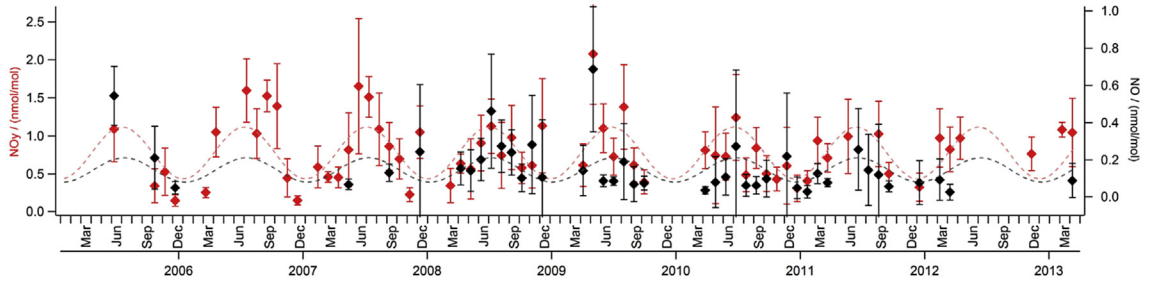

Fig. 6. Nine-year time series of tropospheric NO_y (red, left axis) and NO (black, right axis) measurements over Europe. The data is averaged over one month. The bars denote the standard deviation. For a better illustration of the seasonal cycle, sine functions (dashed lines) are fitted to the data.

CARIBIC likely measures NO_y and NO mixing ratios attributed to lightning NO_x emissions. As an example of the origin of the air

masses encountered over North America, trajectories starting in the North America box for two flights to Vancouver and Denver in July 2008 and July 2009 are shown in Fig. 7 (a). The air masses originated from the north west of the North American continent, from Asia, and from the Pacific. Thunderstorms in the northern part of Canada are less frequent than in the south eastern part of the USA (Orville et al., 2002; Zipser et al., 2006; Cooper et al., 2009; Ridley et al., 2004). Commercial aircraft typically detour thunderstorm clouds. However, outflow air masses with NO_x produced by lightning are encountered. Gressent et al. (2014) investigated with MOZAIC data the influence of lightning NO_x emissions on large scale plumes of NO_x. They showed that 6% of the total MOZAIC NO_y dataset are attributed to lightning NO_x emissions. Most of the large scale NO_x plumes were recorded over North America and the Atlantic mainly in spring and summer during the maximum lightning activity occurrence.

Jaeglé et al. (1998) found that during the SUCCESS mission in April/May 1996 (over the central United States, out of Salina/Kansas), the majority of NO_y in the tropopause region (8–12 km) over the central USA was transported there by convection from the boundary layer. Lightning and aviation only accounted for a small fraction of NO_y. This shows that the upper tropospheric nitrogen oxide budget in North America strongly depends on its geographical location. During SUCCESS, 0.03 nmol/mol NO and 0.27 nmol/mol NO_y were observed at between 8 and 10 km on average. This is only a third (NO only an eighth) of NO_y measured during CARIBIC (cf. Fig. 2 (a)).

Fig. 3 (a) shows the scatter plot between tropospheric NO_y and CO in North America. NO_y reaches roughly up to 2.4 nmol/mol and CO ranges between 55 nmol/mol and 150 nmol/mol. This scatter plot is quite compact, which could also be a consequence of the low amount of available data for this region. Following the previous definition, three CO regimes are defined (see Table 2). Fig. 4 a (light blue) shows the fraction of NO_y measured along with high CO air. On an annual average ~14% of NO_y was measured in high CO air. The NO_y mixing ratio in spring and summer is higher in high CO air than in median or low CO air (Fig. 5).

The fraction of lofted polluted air masses from the boundary layer based on the CO classification is comparable to Europe.

4.1.4. North Atlantic (12°W–53°W, 66°N–40°N)

Fig. 2 (b) shows the NO, NO_y, NO_x, and CO seasonal cycle over the North Atlantic. The data was obtained along the flight tracks between Frankfurt and Vancouver/Canada, Toronto/Canada, Denver/USA, Chicago/USA, Houston/USA, Caracas/Venezuela, and São Paulo/Brazil. Besides ship traffic emissions, the North Atlantic region has no boundary layer sources. In addition to local sources such as aviation, it is influenced by the outflow of polluted air masses from North America (Cooper et al., 2001). NO_y shows a seasonal cycle with a maximum in June (~1.74 nmol/mol) and a minimum in January (~0.27 nmol/mol). The NO seasonal cycle also shows a maximum in June (~0.32 nmol/mol) and a minimum in January (~0.05 nmol/mol). As in North America the mixing ratios decrease sharply after the maximum. During SONEX (Subsonic assessment: Ozone and NOx Experiment), NO and NO_y were measured over the North Atlantic flight corridor (40°N – 60°N) in October and November 1997 (Singh et al., 1999; Jaeglé et al., 1999). They found median values of 0.43 nmol/mol NO_y in tropospheric air (Thompson et al., 1999; Talbot et al., 1999). This is comparable to the present dataset (cf. Fig. 2 (b)).

During the POLINAT 2 aircraft field campaign (Pollution From Aircraft Emissions in the North Atlantic Flight Corridor 2) in September and October 1997, the NO, NO_x, and NO_y distributions in the upper troposphere and lowermost stratosphere over the eastern North Atlantic were measured (Schlager et al., 1997; Ziereis et al., 2000). At between 10 and 12 km altitude and 49°N and 57°N, NO_y mixing ratios between 0.33 nmol/mol and 1.03 nmol/mol and NO mixing ratios between 0.04 nmol/mol and 0.13 nmol/mol were observed. These values are comparable to the present dataset (cf. Fig. 2 (b)). As an example of the origin of the polluted air masses over the North Atlantic, Fig. 7 (b) shows back-trajectories starting at the CARIBIC flight route in the North Atlantic box for two flights to Caracas in July 2009 and July 2010. The air masses originate from the North American continent, from the North American east coast, from the North Atlantic, and from Europe. There are two possible explanations for higher NO_y mixing ratios in summer over the North Atlantic than over North America. A higher strength of the sources in the origin of the air masses (east coast and south east coast vs. west coast and north west coast of North America, cf.

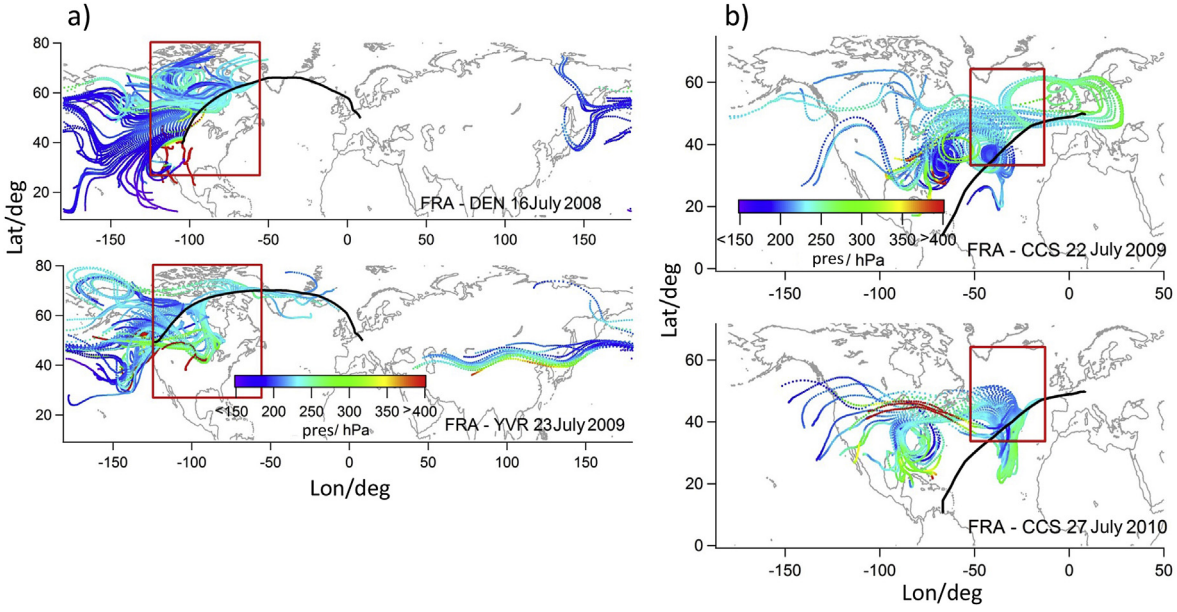

Fig. 7. Flights from Frankfurt to Denver in July 2008 and 2009 (a) and flights from Frankfurt to Caracas in July 2009 and 2010 (b). 5-day backward trajectories, starting in the North Atlantic (a) and North America (b) box (red boxes, see Table 1) are shown. The pressure is color-coded.

Fig. 7), and aviation emissions in the North Atlantic Flight corridor (Grewe, 2007).

Fig. 3 (b) shows the tropospheric NO_y and CO scatter plot over the North Atlantic. NO_y reaches up to 4 nmol/mol and CO ranges between 55 nmol/mol – 280 nmol/mol (in summer, not shown because of the chosen axis scale).

Median CO is given in Table 2. Low, median, and high CO air masses are defined as described above. Fig. 4 a (green) shows that on an annual average ~ 22% of NO_y was detected in high CO air. The fraction of NO_y observed in high CO air in spring is higher than over Europe, North America, and North Asia. Fig. 5 shows, that in general highest mean NO_y mixing ratios were detected in high CO air masses.

4.1.5. Arctic (160°W – 160°E, 66°N – 90°N)

Fig. 2 (e) shows the NO, NO_y, NO_x, and CO seasonal cycle in the Arctic. The data was obtained along the flight tracks between Frankfurt and Osaka/Japan and Vancouver/Canada. The tropopause height decreases at higher latitudes, therefore most of the data during these flights was obtained in the lower stratosphere. Only ~11% of all data in this region was obtained in the troposphere. NO and NO_y show a similar seasonal cycle with a maximum in June (NO_y: ~0.96 nmol/mol, NO: ~0.28 nmol/mol), a NO_y minimum in February (~0.36 nmol/mol), and a NO minimum in April (~0.04 nmol/mol).

The Arctic has sparse local NO and NO_y sources. The trace gas distribution in this region is controlled by long-range transport (including biomass burning plumes, anthropogenic plumes) (Law et al., 2014). Polluted air masses from the mid-latitudes are transported to the Arctic. This results in the so called Arctic haze, an aerosol maximum in spring/summer that also shows elevated levels of nitrogen oxides (Law et al., 2014). POLARCAT (Polar Study using Aircraft, Remote Sensing, Surface Measurements and Models, of Climate, Chemistry, Aerosols, and Transport) data showed that fire emissions (agricultural and boreal) and anthropogenic emissions from East Asia contribute to the trace gas and aerosol distribution observed over the Arctic in spring and summer 2008 (Law et al., 2014).

Singh et al. (2010) found that pollution plumes were transported to the Arctic region from Europe and Asia during the NASA ARCTAS-A (spring) and ARCTAS-B (summer) campaign in 2008 (Arctic Research of the Composition of the Troposphere from Aircraft and Satellites). The plumes were present in the mid to upper troposphere and contained a mix of forest fire and urban influences.

Furthermore, Liang et al. (2011) identified stratosphere-troposphere-exchange (STE) and anthropogenic and biomass burning emissions as the main source of NO_y in the troposphere during ARCTAS-A and -B. In the middle troposphere combustion plumes are the major contributors of NO_y, whereas in the upper troposphere (>6 km) STE and biomass burning contribute significantly to NO_y. Furthermore, they found that convection and/or lightning influences are negligible sources in the Arctic troposphere but can have significant impacts in the upper troposphere in the continental sub-Arctic during summer. Liang et al. (2011) found in background air (6–12 km) ~ 0.009 nmol/mol NO and ~0.39 nmol/mol NO_y during ARCTAS-A, and ~0.01 nmol/mol NO and ~0.37 nmol/mol NO_y during ARCTAS-B. Their findings are in agreement with the CARIBIC measurements (see Fig. 2 (e)). Fig. 3 (e) shows the NO_y and CO scatter plot. The majority of the data ranges between 70 and 140 nmol/mol CO and reaches NO_y values up to 2.5 nmol/mol. The highest NO_y mixing ratios were found in the summer months along with CO mixing ratios of around 90–100 nmol/mol.

Median CO mixing ratios in the Arctic are given in Table 2. Fig. 4 a (red) shows that on annual average ~ 8% of NO_y was detected in high CO air.

4.2. NO and NO_y mixing ratios between 25°N and 40°S: South Asia West, South Asia East, sub/tropical Atlantic, Africa, and South America

4.2.1. South Asia West (45°E–99°E, 10°N–35°N)

The chemical composition of the upper troposphere in South Asia is influenced by the monsoon. A large amount of polluted boundary layer air is transported to the tropopause region in the western part over India (Schuck et al., 2010; Baker et al., 2011; Rauthe-Schöch et al., 2015). Furthermore, Lai et al. (2010) and Baker et al. (2014), observed high-pollution events in the tropopause region in Southeast Asia. Therefore, we have split the data in South Asia into a western and an eastern part. Fig. 2 (i) shows the seasonal cycle of NO_y, NO, NO_x and CO in South Asia W. The data was obtained along the flight tracks between Frankfurt and Chennai/India. The NO_y mixing ratios show a seasonal cycle that differs from the seasonal cycles in Europe, North Asia, North Atlantic, and North America. The seasonal cycle features two maxima, which are located in May and September (~0.95 nmol/mol). In between, the mixing ratio decreases to ~0.51 nmol/mol in August. The minimum is located in November (0.34 nmol/mol). NO shows a similar seasonal cycle with low mixing ratios in the summer months (~0.12 nmol/mol).

Similar observations were made during NOXAR and POLINAT 2 (Brunner et al., 2001). Maxima in NO_x were observed in spring and autumn in Southeast Asia (10°N–30°N, 70°E–120°E). Brunner et al. (2001) argued that this pattern is connected to the Indian summer monsoon, where unstable atmospheric layering causes rainfall (Krishnamurti and Bhalme, 1976). Due to high temperatures and high OH mixing ratios, oxidation from NO_x to HNO_3 is promoted and can be removed by rainout or washout.

Satellite-derived (Ozone Monitoring Instrument, OMI) NO_2 columns over rural regions in India capture rain-induced soil NO_x pulses during the onset of the rainy season (June) and a subsequent decrease during the break spell of precipitation (Ghude et al., 2010). This is not in contrast to our observations (decreasing NO_y in June), because high temperatures and high OH mixing ratios promote oxidation from NO_x to HNO_3. HNO_3 can be removed during transport processes by rainout.

Lal and Pawar (2009) showed a correlation between lightning frequency and convective rainfall during the monsoon and the premonsoon period over the central Indian region. With TRMM (Tropical Rainfall Measuring Mission) satellite data they showed that the number of lightning flashes per month is highest in May (~2780). From May until August the number decreases (~1000 lightning flashes/month). In September there is a second maximum in the number of lightning flashes (~2000). However, the total rainfall has a nearly constant maximum from June until September (~0.23 mm/h). The two NO_y maxima in May and September could be a result of the number of lightning flashes.

In contrast to HNO_3 and its water solubility, greenhouse gases and non-methane hydrocarbons (NMHC) show a different behavior during the monsoon period. During the CARIBIC flights in 2008 to Chennai/India, Schuck et al. (2010) observed the formation of a monsoon plume with enhanced mixing ratios of CH_4, N_2O, SF_6, CO, and H_2O. The plume developed in May and persisted through September. Maximum mixing ratios and maximum spatial extension of the plume were observed in August. Baker et al. (2011) found evidence for the influence of convectively uplifted boundary layer air, indicated by large enhancements in the mixing ratios of NMHC in the upper troposphere over southwestern Asia during the monsoon.

Fig. 3 (i) shows the scatter plot between tropospheric NO_y and

CO in South Asia W. NO_y reaches values up to 5 nmol/mol (not shown because of the chosen axis scale), while the majority of CO ranges between 55 nmol/mol and 170 nmol/mol.

Median CO mixing ratios in South Asia W are shown in Table 2. Fig. 4 b (green) shows that on annual average ~ 19% of NO_y was detected in high CO air. The highest fraction of NO_y observed in high CO air is found in spring. During this season NO_y might originate partly from biomass burning, which is most frequent in spring in South Asia (Dwyer et al., 2000). Mean NO_y mixing ratios detected in high CO air are higher than in low and median CO air (Fig. 5).

4.2.2. South Asia East (99°E, 125°E, 0°N–35°N)

In South Asia E, the data was obtained along the flight tracks between Frankfurt and Guangzhou/China and Bangkok/Thailand, as well as during the connecting flights between Bangkok/Thailand and Kuala Lumpur/Malaysia and between Guangzhou/China and Manila/the Philippines. Flights to Guangzhou and Manila where conducted from 2005 to 2008. The chemical composition of the upper troposphere in South Asia E is influenced by the monsoon (Rauthe-Schöch et al., 2015), and by strong biomass burning events (Lai et al., 2010; Lelieveld et al., 2001; Kondo et al., 2004).

Fig. 2 (j) shows the NO, NO_y, NO_x, and CO seasonal cycle in South Asia E. NO and NO_y show similar seasonal cycles, with maximum mixing ratios in May (NO_y: ~0.93 nmol/mol, NO: 0.42 nmol/mol), minimum NO_y mixing ratios in November (~0.3 nmol/mol), and minimum NO mixing ratios in December (~0.12 nmol/mol), respectively.

During PEM-West A (Pacific Exploratory Mission-West A), 0.06 nmol/mol NO and 0.59 nmol/mol NO_y were observed in the outflow from the Asian continent between September and October 1991 over the western Pacific Ocean (Talbot et al., 1996). NO_y observed within CARIBIC is comparable to the values observed during PEM-West A, but measured NO is considerably less (cf. Fig. 2 (j)). During PEM-West-A, observations were performed in the outflow from the Asian continent, where a fraction of NO is already chemically transformed. CARIBIC measurements were performed closer to the sources.

Fig. 3 (j) shows the scatter plot between tropospheric NO_y and CO in South Asia E. NO_y reaches values up to 8 nmol/mol in spring (not shown because of the chosen axis scale). The CO values range between 55 nmol/mol and 280 nmol/mol. Enhanced NO_y along with enhanced CO is observed in each season. This indicates a strong influence from boundary layer pollution on the NO_y budget in the upper troposphere. Lai et al. (2010) analyzed CARIBIC flights from April 2007 over South China and the Philippines (flights to Guangzhou and Manila). They found strong pollution episodes in the upper troposphere, with enhancements in aerosol and trace gas concentrations including CO, CO_2, CH_4, NMHC, and halocarbons. They concluded that biomass/biofuel burning in Mainland Southeast Asia was the main source of the pollution plumes.

Median CO mixing ratios in South Asia E can be found in Table 2. Low, median, and high CO air masses are defined as described above. Fig. 4 b (dark blue) shows that on annual average ~ 25% of NO_y was detected in high CO air masses. The highest fraction of NO_y in high CO air is observed in autumn. Compared to South Asia W, the fraction of NO_y measured in high CO air masses is higher in summer and autumn and about the same in spring and winter (see Fig. 4 b (green and dark blue)). In the region described above, highest mean NO_y mixing ratios were found in high CO air masses (Fig. 5).

4.2.3. South America (75°W – 28°W, 3°S – 35°S)

Fig. 2 (g) shows NO, NO_y, NO_x, and CO data from South America. The data was obtained along the flight tracks between Frankfurt and São Paulo/Brazil and the connecting flights between São Paulo and Santiago de Chile/Chile in 2005 and 2006. Observations in this region were only carried out over five months, so no complete seasonal cycle can be shown. The maximum NO_y concentration was observed in October with ~1.37 nmol/mol. The minimum is in February with ~0.22 nmol/mol. NO shows a similar behavior with a maximum in October (~0.27 nmol/mol) and a minimum in June (~0.04 nmol/mol). The region of South America is covered in large part with rainforest. Biomass burning and lightning are the main sources for nitrogen oxides (Ebinghaus et al., 2007; Huntrieser et al., 2007).

Fig. 3 (g) shows the scatter plot between tropospheric NO_y and CO. In spring (northern hemispheric definition, MAM) and winter (DJF), NO_y mixing ratios reach up to 2–3 nmol/mol, while CO mixing ratios are around 60–100 nmol/mol. In autumn (northern hemispheric definition), NO_y reaches up to 4 nmol/mol and the majority of the data ranges between 50 nmol/mol and 350 nmol/mol CO. Note the remarkable positive correlation between NO_y and CO in autumn. This indicates that biomass burning causes the emission of nitrogen oxides. Note that in autumn only two flights were made to South America. Ebinghaus et al. (2007) showed that the two flights in autumn 2005 were influenced by forest fires in Brazil in October, using mercury as a tracer for biomass burning.

Median CO mixing ratios in South America are listed in Table 2. Median CO for autumn is strongly influenced by the above-mentioned biomass burning events and might therefore not be representative for this region and season.

Fig. 4 b (purple) shows the fraction of NO_y measured along with high CO air. On annual average ~27% of NO_y was detected high CO air. The fraction of NO_y measured in high CO air was highest in autumn (45%). In comparison to the other southern regional boxes, this is the highest amount of NO_y measured in high CO air masses.

4.2.4. Sub/Tropical Atlantic (12°W – 60°W, 30°N – 5°S)

Fig. 2 (h) shows the NO, NO_y, NO_x, and CO seasonal cycle over the tropical Atlantic. The data in this region was obtained along the flight tracks between Frankfurt and Caracas/Venezuela and São Paulo/Brazil. Except for ship traffic, the Tropical Atlantic is a region without ground-based nitrogen oxide sources. The air traffic density is considerably lower than in the North Atlantic flight corridor (Eyers et al., 2005).

NO_y shows a seasonal cycle with a maximum in July (~0.8 nmol/mol) and a minimum in November (~0.2 nmol/mol). The NO mixing ratio ranges between 0.08 nmol/mol in January and 0.18 nmol/mol in July. NO_y reaches values up to 2.8 nmol/mol in summer (northern hemispheric definition, JJA) (Fig. 3 (h)). The majority of the CO values range between 55 nmol/mol and 145 nmol/mol. The positive NO_y-CO correlation in autumn is caused by the same biomass burning plume that was observed in autumn 2005 over South America. This indicates that the outflow from South America influences the UT over the Sub/Tropical Atlantic.

Median CO mixing ratios over the Sub/Tropical Atlantic are listed in Table 2. On annual average ~20% of NO_y was detected in high CO air masses (see Fig. 4 b (light blue)).

4.2.5. Africa (0°E–35°E, 20°N–35°S)

Fig. 2 (f) shows the NO, NO_y, NO_x, and CO seasonal cycle in Africa. The data in this region was obtained along the flight routes to Cape Town/South Africa and Johannesburg/South Africa. Altogether 13 flights were made between Germany and South Africa. No flights were made during the summer months of June, July, and August, so no complete seasonal cycle can be shown. The regional box covers various latitudes with different sources. Therefore, Fig. 8 shows the NO and NO_y mixing ratios along latitude. In spring (northern hemispheric definition, MAM), NO_y reaches its maximum at around 5°N – 25°N (~2.00 nmol/mol); in autumn, the maximum NO_y

mixing ratio is reached around 0°–10°S (~1.50 nmol/mol); in winter, the NO_y maximum is around 5°N – 5°S (~1.50 nmol/mol). This is in contrast to the expected mixing ratios.

Previous studies (Roberts et al., 2009) showed that the main burning regions in central Africa move throughout the year from the northern hemisphere (around 5°N–15°N, September through March) to the southern hemisphere (around 10°S – 20°S, April through August). Based on different emission inventories, the monthly CO budget in Africa is highest in July, and lowest between March and April (Liousse et al., 2010). The Inter-Tropical Convergence Zone (ITCZ) moves northward (July) and southward (January) from the equator. This in turn influences the region with the strongest convection and thus thunderstorms.

Fig. 3 (f) shows the scatter plot of the seasonal relationship between tropospheric NO_y and CO in Africa. NO_y reaches mixing ratios of up to 6 nmol/mol (not shown because of the chosen axis scale) in a CO range between 50 and 250 nmol/mol. During all seasons, enhanced NO_y is observed along with enhanced CO, which indicates a strong influence from the boundary layer. High NO_y mixing ratios are also observed, with no concurrent enhancement of CO. This hints at lightning as a source of NO_y. CO mixing ratios (~150 nmol/mol) exceeding background CO (~80–100 nmol/mol) could be caused by the strong convective activity throughout the year. This is supported by backward trajectories that show rapid uplift in this region (not shown), indicative of convection. That a variety of sources (biomass burning, lightning, and anthropogenic emissions) contribute to the NO_y budget over Africa was also shown by Richter and Burrows (2002) with GOME (Global Ozone Monitoring Experiment) satellite measurements in autumn 1997.

Table 2 shows median CO mixing ratios in Africa. Fig. 4 b (red) shows that ~ 38% NO_y was measured in high CO air on annual average. Fig. 5 shows that mean NO_y mixing ratios were highest when detected in high CO air masses.

4.3. Summary of the NO and NO_y mixing ratios in the regional boxes

For a better comparison of the data obtained in the different regional boxes, the NO and NO_y mixing ratios have been averaged over all seasons (Figs. 9 and 10, and Tables 3 and 4). This representation allows a clear comparison of the mean and median NO and NO_y mixing ratios. On annual average, the highest NO and NO_y mixing ratios were found over Africa (~0.23 nmol/mol NO and ~1.12 nmol/mol NO_y). The lowest annual averages were observed over the Sub/Tropical Atlantic (~0.50 nmol/mol NO_y) and in the Arctic (~0.08 nmol/mol NO). In the regions north of 40°N, NO_y shows a clear seasonal cycle with a maximum in summer and a minimum in winter (except for North America). The seasonal cycles are conceivably the consequence of the higher lightning intensity and higher convective activity in the summer months.

The highest fraction of NO_y in high CO air masses in Europe, North Asia, and North America was found in summer; presumably a consequence of the higher convective activity. The mean NO_y mixing ratios are in general highest when detected in high CO air masses (Fig. 5).

There is no consistent seasonal dependence for all regional boxes <40°N. Here nitrogen sources such as biomass burning (South America), the monsoon (South Asia), and the strong convection at the ITCZ (Africa) strongly influence the unique NO_y seasonal cycle.

Comparing the mean and median NO and NO_y values in Figs. 9 and 10 and in Tables 3 and 4, it is noticeable that the mean values are generally higher than the median values. This likely shows the significance of some high mixing ratios, induced by lightning, convection, and perhaps – though to a smaller extent – aircraft emissions.

5. Comparison with nitrogen oxide data from other in-service aircraft measurements

There are numerous field campaigns involving research aircraft that were dedicated to the observation of nitrogen oxides in the troposphere. Most of these measurement efforts have been focused on specific scientific questions. In any case these field campaigns have restricted time and regional coverage. Taking into account the variety of nitrogen oxide sources in combination with their short lifetime, comparing these measurements with the CARIBIC dataset is difficult. Therefore, a comparison with data obtained from similar programs is more suitable. Here we compare the CARIBIC data with measurements performed within the MOZAIC (Volz-Thomas et al., 2005; Thomas et al., 2015) and NOXAR/POLINAT (Brunner et al., 2001) programs, respectively.

Within the framework of NOXAR, NO, NO_2, and O_3 were measured between May 1995 and May 1996 onboard a Swissair passenger aircraft B747-357 during 540 flights (Brunner et al., 2001). Between August and November 1997 these measurements were conducted within the framework of POLINAT 2 during 104 flights. NO was measured using a chemiluminescence technique. NO_2 was calculated using measured NO and O_3 and a modeled photolysis rate assuming a photostationary steady state. The time resolution was 2 min.

For the comparison between calculated NOXAR/POLINAT 2 NO_x and calculated CARIBIC NO_x, the CARIBIC data was grouped into the same four regions, as defined in (Brunner et al., 2001): Europe/Asia (40°N–65°N, 10°E–120°E), S/E Asia (10°N–30°N, 70°E–120°E), North Atlantic (40°N–60°N, 10°W–40°W) and North America

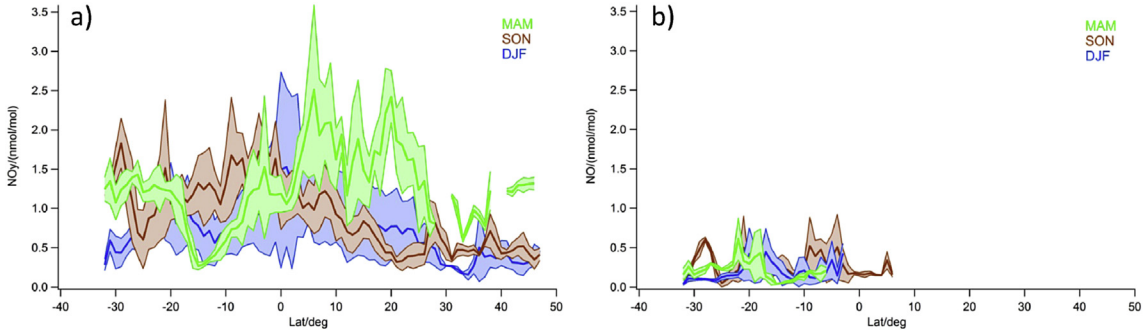

Fig. 8. NO_y (a) and NO (b) along the flight routes to Cape Town/South Africa and Johannesburg/South Africa in spring (MAM, in this case only March), autumn (SON, in this case only October and November), and winter (DJF). The data is averaged over latitude bins of 1°. The shaded area shows the standard deviation.

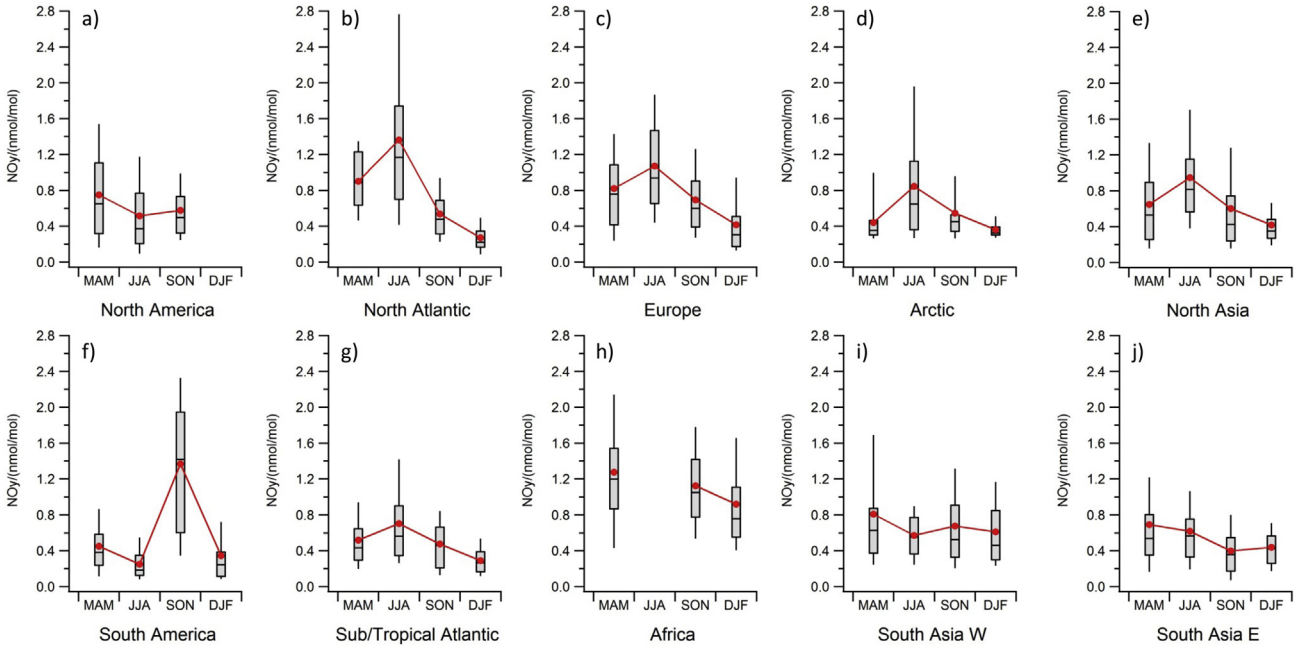

Fig. 9. Mean and median tropospheric NO_y mixing ratios between 2005 and 2013. The data is averaged over regions and seasons. Black markers: mean. Boxplots contain median, quartiles, and deciles.

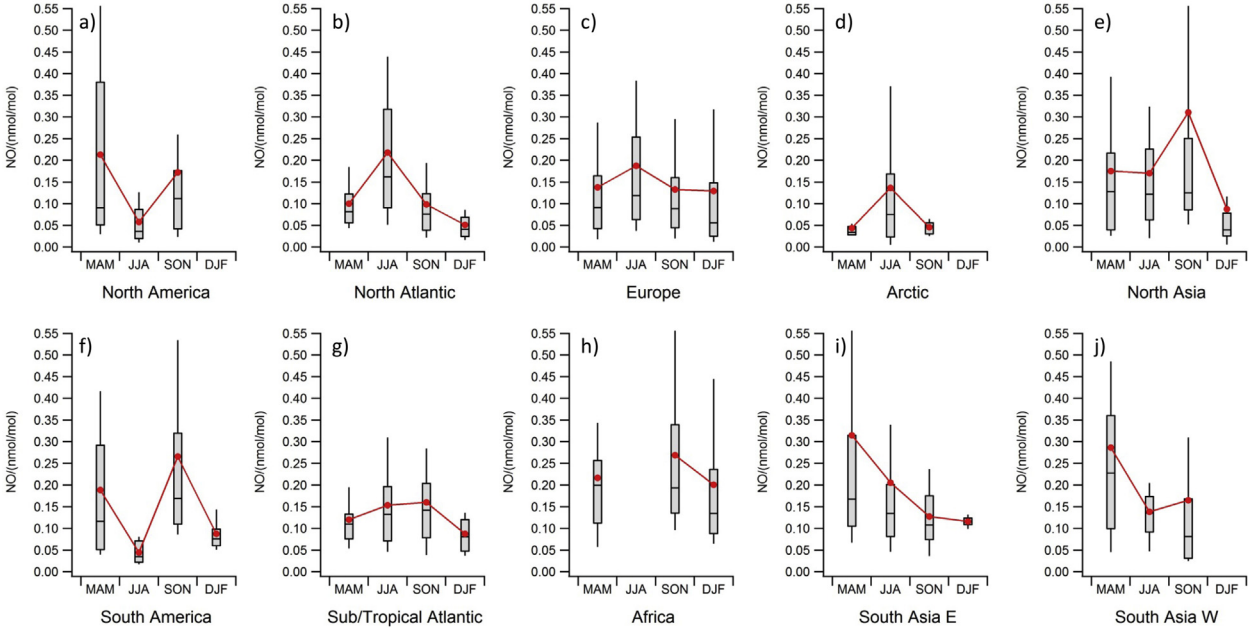

Fig. 10. Same as Fig. 9, but for NO. The $Q_{0.9}$ decile in North Asia in SON is 1.13, and 0.69 in South Asia E in MAM.

(35°N–60°N, 60°W–100°W). Only tropospheric data points were used for this analysis. Fig. 11 shows the median NO_x mixing ratios in the four regions. The seasonal cycle of both datasets is similar in Europe/Asia and over the North Atlantic, with maximum mixing ratios in summer and minimum mixing ratios in winter/spring. Generally, CARIBIC NO_x is higher than NOXAR/POLINAT 2 NO_x (on annual average ~ 0.08 nmol/mol (~49%) in Europe/Asia). The strongest discrepancies were found in spring and summer over North America (~0.2 nmol/mol, respectively). Brunner et al. (2001) explain the high NO_x mixing ratios (the highest mixing ratios of all regions) with enhanced lightning activity and convective processes in the south eastern part of the USA. Cooper et al. (2009) also found that the majority of summertime NO_x in the eastern and southern part of the USA is produced from lightning. Orville et al., (2002) evaluated lightning data from the North American Lightning Detection Network (NALDN) between 1998 and 2000. The highest lightning frequencies were found along the Gulf of Mexico and Florida (exceeding 9 flashes per km^2). Cooper et al. (2009) calculated that lightning is the source of approx. 80% of upper tropospheric nitrogen oxides over the eastern USA. The discrepancy with the CARIBIC data can be explained by the fact that the CARIBIC flight paths are mainly located in the northern part of this region and

Table 3
Tropospheric NO_y mixing ratios (nmol/mol) between 2005 and 2013, averaged over seasons and region.[a]

Season	Region	Mean ± stdev	Median	n	Region	Mean ± stdev	Median	n
MAM	North	0.75 ± 0.486	0.652	1007	South	0.449 ± 0.3	0.382	2628
JJA	America	0.515 ± 0.399	0.374	1058	America	0.251 ± 0.178	0.184	1280
SON		0.578 ± 0.369	0.498	2988		1.367 ± 0.768	1.416	2435
DJF		–	–	0		0.345 ± 0.378	0.243	4515
MAM	North	0.903 ± 0.353	0.89	2492	Tropical	0.517 ± 0.325	0.431	6924
JJA	Atlantic	1.36 ± 0.858	1.167	3975	Atlantic	0.705 ± 0.489	0.563	7958
SON		0.539 ± 0.298	0.479	6583		0.477 ± 0.305	0.459	9085
DJF		0.273 ± 0.183	0.221	2597		0.292 ± 0.151	0.267	5961
MAM	Europe	0.822 ± 0.54	0.758	5745	Africa	1.274 ± 0.66	1.197	4106
JJA		1.07 ± 0.565	0.94	6972		–	–	0
SON		0.695 ± 0.414	0.6	8914		1.123 ± 0.487	1.05	5495
DJF		0.416 ± 0.362	0.305	4865		0.921 ± 0.566	0.756	11,316
MAM	Arctic	0.442 ± 0.257	0.354	207	South	0.808 ± 0.712	0.628	12,118
JJA		0.847 ± 0.616	0.648	744	Asia W	0.571 ± 0.277	0.552	9600
SON		0.545 ± 0.389	0.449	788		0.675 ± 0.494	0.525	10,732
DJF		0.361 ± 0.098	0.324	702		0.61 ± 0.408	0.459	5415
MAM	North	0.648 ± 0.506	0.532	8122	South	0.691 ± 0.704	0.537	8581
JJA	Asia	0.948 ± 0.605	0.815	9532	Asia E	0.618 ± 0.461	0.564	5420
SON		0.601 ± 0.527	0.427	6124		0.398 ± 0.278	0.359	5591
DJF		0.419 ± 0.369	0.352	3498		0.437 ± 0.23	0.424	2978

[a] n: number of 10 s averaged samples.

Table 4
As Table 3, but for NO.[a]

Season	Region	Mean ± stdev	Median	n	Region	Mean ± stdev	Median	n
MAM	North	0.213 ± 0.232	0.09	739	South	0.189 ± 0.17	0.116	1147
JJA	America	0.058 ± 0.053	0.036	1543	America	0.044 ± 0.026	0.033	428
SON		0.172 ± 0.265	0.112	1820		0.265 ± 0.27	0.169	832
DJF		–	–	0		0.087 ± 0.055	0.076	1045
MAM	North	0.1 ± 0.07	0.081	2269	Tropical	0.12 ± 0.075	0.11	1740
JJA	Atlantic	0.217 ± 0.166	0.162	3696	Atlantic	0.153 ± 0.108	0.132	3949
SON		0.098 ± 0.097	0.076	2912		0.16 ± 0.127	0.142	4015
DJF		0.051 ± 0.041	0.041	1478		0.087 ± 0.044	0.081	1604
MAM	Europe	0.138 ± 0.164	0.091	4124	Africa	0.216 ± 0.169	0.2	1049
JJA		0.187 ± 0.209	0.119	3973		–	–	0
SON		0.133 ± 0.166	0.089	3361		0.269 ± 0.218	0.193	2364
DJF		0.129 ± 0.235	0.056	2022		0.201 ± 0.178	0.135	3085
MAM	Arctic	0.044 ± 0.045	0.034	168	South	0.286 ± 0.527	0.228	2219
JJA		0.136 ± 0.157	0.075	633	Asia W	0.139 ± 0.088	0.135	2069
SON		0.046 ± 0.015	0.049	107		0.165 ± 0.276	0.081	2558
DJF		–	–	0		–	–	0
MAM	North	0.175 ± 0.206	0.128	3120	South	0.315 ± 0.437	0.167	2940
JJA	Asia	0.17 ± 0.191	0.122	6263	Asia E	0.206 ± 0.336	0.135	2366
SON		0.311 ± 0.438	0.125	1642		0.128 ± 0.077	0.108	1963
DJF		0.087 ± 0.416	0.039	1261		0.116 ± 0.012	0.116	332

[a] n: number of 10 s averaged samples.

therefore are not or less affected by fresh polluted air masses due to lightning and convective processes, which occur more frequently in the South East of the United States than in its northern parts.

MOZAIC NO_y measurements began in May 2001 onboard one Lufthansa Airbus A340-300 passenger aircraft. NO_y mixing ratios through 2005 are available on the MOZAIC website (http://www.iagos.fr/extract/). The measurements were conducted using a chemiluminescence technique and a catalytic gold converter (Volz-Thomas et al., 2005). The permanently installed instrument was maintained every four to six weeks. CARIBIC and MOZAIC NO_y data are compared for the Europe region (cf. Table 1). The time resolution of the MOZAIC NO_y measurements was 1 min. For this comparison, only data obtained in the upper troposphere for pressures lower than 500 hPa is used. 235 CARIBIC flights and approx. 1400 MOZAIC flights in the Europe region were compared. Since no PV data is provided for the MOZAIC data, the chemical O_3 tropopause (TP) definition (Zahn et al., 2002) is used to distinguish between tropospheric and stratospheric air masses. The O_3 TP changes with season and latitude. Based on this definition, an average O_3 TP for each season is used: ~119.5 nmol/mol in spring, ~102.9 nmol/mol in summer, ~74.3 nmol/mol in autumn, and ~90.8 nmol/mol in winter.

Fig. 12 shows the mean and median NO_y volume mixing ratios of both datasets. In spring and autumn CARIBIC NO_y is ~0.06 nmol/mol higher than MOZAIC NO_y. In summer and winter MOZAIC NO_y is ~0.02 nmol/mol higher. On annual average, these two datasets show a difference of ~7%. CARIBIC and MOZAIC NO_y mixing ratios in the UT over Europe are consistent with each other.

6. Concluding remarks

Between May 2005 and April 2013, NO and NO_y measurements were performed aboard a passenger aircraft within the framework of CARIBIC. This dataset is the longest NO and NO_y dataset available today for the upper troposphere. The dataset covers the region

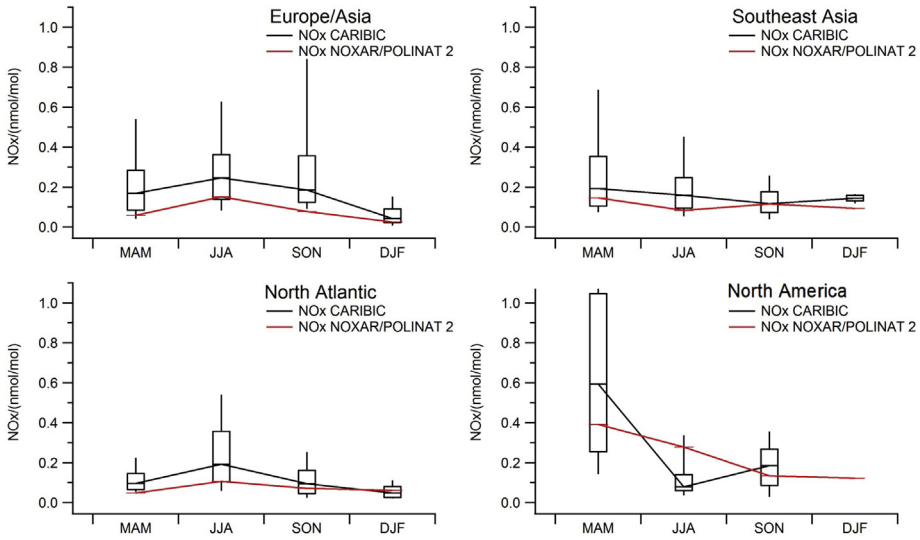

Fig. 11. Comparison between tropospheric CARIBIC NO_x (2005–2013) and NOXAR/POLINAT 2 NO_x (1995–1996, 1997). CARIBIC NO_x boxplots contain median, quartiles, and deciles. Median NOXAR/POLINAT 2 NO_x is taken from Brunner et al. (2001).

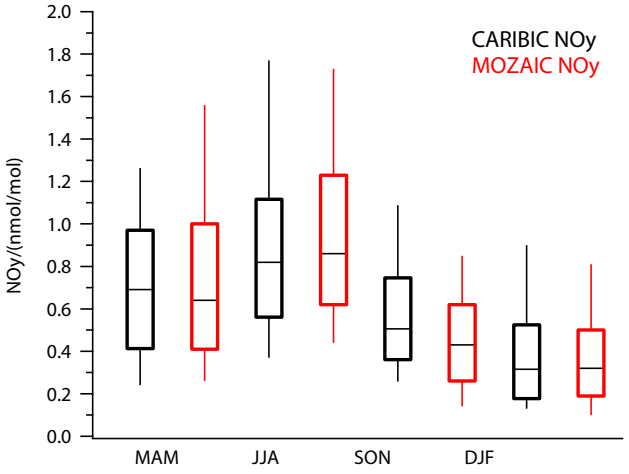

Fig. 12. Comparison between tropospheric CARIBIC NO_y (2005–2013) (black) and MOZAIC NO_y (2001–2005) (red) in Europe. Boxplots contain median, quartiles, and deciles.

between 124°W and 142°E and between 77°N and 35°S and was measured in heights of between 500 hPa and 180 hPa.

In the regions north of 40°N (North Atlantic, Europe, Arctic, and North Asia), clear NO_y seasonal cycles with maxima in summer and minima in winter are observed. The NO seasonal cycles are less clear. They show maxima in summer (North Atlantic, Europe, and Arctic), autumn (North Asia), and spring (North America). The NO_y (NO) mixing ratios range between 1.36 (0.22) nmol/mol in summer and 0.27 (0.05) nmol/mol in winter.

For the regions south of 40°N (South America, Sub/Tropical Atlantic, Africa, South Asia W, and South Asia E), no uniform seasonal dependence was observed. The NO_y (NO) mixing ratios range between 1.37 (0.32) nmol/mol and 0.29 (0.04) nmol/mol. The seasonal cycles shown here are strongly influenced by biomass burning (South America), the monsoon (South Asia), and the strong convection at the ITCZ (Africa).

On annual average, the highest NO and NO_y mixing ratios were found in Africa (~0.23 nmol/mol NO and ~1.12 nmol/mol NO_y). The lowest annual averages were observed over the Sub/Tropical Atlantic (~0.50 nmol/mol NO_y) and in the Arctic (~0.08 nmol/mol NO).

The observed mean NO and NO_y values are consistent with values obtained during several other aircraft campaigns.

Low, median, and high CO air masses were defined. In the regions >40°N 2%–34% of the measured NO_y data was obtained in high CO air masses. Generally, more data was obtained in high CO air masses in the regions south of 40°N (19%–38%) compared to the northern regions. This indicates that here NO_y in the upper troposphere more often originates from polluted boundary layer sources than in the northern regions.

In the northern regions (>40°N) the majority of NO_y measured in high CO air masses was observed in summer (except over the North Atlantic and the Arctic), presumably a consequence of the higher convective activity, and in the southern regions (<40°N) in autumn (northern hemispheric definition, SON) and winter (except for Africa). If NO_y was measured along with high CO air masses, NO_y mixing ratios are in general higher than in median or low CO air masses.

The CARIBIC NO and NO_y measurements provide a good approximation to upper tropospheric NO and NO_y climatological mean distributions. Small scale NO and NO_y enhancements caused by air traffic alter the average concentration only marginal. Fresh aircraft plumes account for only ~ 0.9% of the entire NO and NO_y measurement period. A negative bias due to avoiding flying through thunderstorms is not expected, because the air masses in the outflow of thunderstorm clouds are encountered. Therefore, this dataset is highly suitable for the validation of atmosphere-chemistry models.

IAGOS-CARIBIC nitrogen oxide measurements will be continued.

Acknowledgments

CARIBIC data is available from the CARIBIC team (see http://www.caribic-atmospheric.com/) on signing the CARIBIC data protocol. This work was supported by the Federal Ministry of Education and Research under the project number 01LK1223E within the pilot phase IAGOS-D, and by the DLR-project WeCare. We wish to thank Lufthansa and Lufthansa Technik for their ongoing support as well as all CARIBIC partners. We especially acknowledge D. Scharffe,

C. Koeppel, and S. Weber for the operation of this complex platform.

References

Baker, A.K., Schuck, T.J., Slemr, F., van Velthoven, P., Zahn, A., Brenninkmeijer, C.A.M., 2011. Characterization of non-methane hydrocarbons in Asian summer monsoon outflow observed by the CARIBIC aircraft. Atmos. Chem. Phys. 11 (2), 503–518. http://dx.doi.org/10.5194/acp-11-503-2011.

Baker, A.K., Traud, S., Brenninkmeijer, C.A.M., Hoor, P., Neumaier, M., Oram, D.E., Rauthe-Schöch, A., Sprung, D., Schloegl, S., Slemr, F., van Velthoven, Peter F.J., Wernli, H., Zahn, A., Ziereis, H., 2014. Pollution patterns in the upper troposphere over Europe and Asia observed by CARIBIC. Atmos. Environ. 96 (0), 245–256. http://dx.doi.org/10.1016/j.atmosenv.2014.06.010.

Bertram, T.H., Perring, A.E., Wooldridge, P.J., Crounse, J.D., Kwan, A.J., Wennberg, P.O., Scheuer, E., Dibb, J., Avery, M., Sachse, G., Vay, S.A., Crawford, J.H., McNaughton, C.S., Clarke, A., Pickering, K.E., Fuelberg, H., Huey, G., Blake, D.R., Singh, H.B., Hall, S.R., Shetter, R.E., Fried, A., Heikes, B.G., Cohen, R.C., 2007. Direct measurements of the convective recycling of the upper troposphere. Science 315 (5813), 816–820. http://dx.doi.org/10.1126/science.1134548.

Bollinger, M.J., Sievers, R.E., Fahey, D.W., Fehsenfeld, F.C., 1983. Conversion of nitrogen dioxide, nitric acid, and n-propyl nitrate to nitric oxide by a gold-catalyzed reduction with carbon monoxide. Anal. Chem. 55 (12), 1980–1986. http://dx.doi.org/10.1021/ac00262a034.

Bradshaw, J., Davis, D., Crawford, J., Chen, G., Shetter, R., Müller, M., Gregory, G., Sachse, G., Blake, D., Heikes, B., Singh, H., Mastromarino, J., Sandholm, S., 1999. Photofragmentation two-photon laser-induced fluorescence detection of NO_2 and NO: comparison of measurements with model results based on airborne observations during PEM-Tropics A. Geophys. Res. Lett. 26 (4), 471–474. http://dx.doi.org/10.1029/1999GL900015.

Bradshaw, J., Davis, D., Grodzinsky, G., Smyth, S., Newell, R., Sandholm, S., Liu, S., 2000. Observed distributions of nitrogen oxides in the remote free troposphere from the Nasa global tropospheric experiment programs. Rev. Geophys. 38 (1), 61–116.

Brenninkmeijer, C.A.M., Crutzen, P., Boumard, F., Dauer, T., Dix, B., Ebinghaus, R., Filippi, D., Fischer, H., Franke, H., Frie\beta, U., Heintzenberg, J., Helleis, F., Hermann, M., Kock, H.H., Koeppel, C., Lelieveld, J., Leuenberger, M., Martinsson, B.G., Miemczyk, S., Moret, H.P., Nguyen, H.N., Nyfeler, P., Oram, D., O'Sullivan, D., Penkett, S., Platt, U., Pupek, M., Ramonet, M., Randa, B., Reichelt, M., Rhee, T.S., Rohwer, J., Rosenfeld, K., Scharffe, D., Schlager, H., Schumann, U., Slemr, F., Sprung, D., Stock, P., Thaler, R., Valentino, F., van Velthoven, P., Waibel, A., Wandel, A., Waschitschek, K., Wiedensohler, A., Xueref-Remy, I., Zahn, A., Zech, U., Ziereis, H., 2007. Civil aircraft for the regular investigation of the atmosphere based on an instrumented container: the new CARIBIC system. Atmos. Chem. Phys. 7 (18), 4953–4976. http://dx.doi.org/10.5194/acp-7-4953-2007.

Brenninkmeijer, C.A.M., Crutzen, P.J., Fischer, H., Güsten, H., Hans, W., Heinrich, G., Heintzenberg, J., Hermann, M., Immelmann, T., Kersting, D., Maiss, M., Nolle, M., Pitscheider, A., Pohlkamp, H., Scharffe, D., Specht, K., Wiedensohler, A., 1999. CARIBIC – civil aircraft for global measurement of trace gases and aerosols in the Tropopause region. J. Atmos. Ocean. Technol. 16 (10), 1373–1383. http://dx.doi.org/10.1175/1520-0426(1999)016<1373:CCAFGM>2.0.CO;2.

Brunner, D., Staehelin, J., Jeker, D., Wernli, H., Schumann, U., 2001. Nitrogen oxides and ozone in the tropopause region of the northern hemisphere: measurements from commercial aircraft in 1995/1996 and 1997. J. Geophys. Res. 106 (D21), 27673–27699.

Buhr, M., Parrish, D.D., Elliot, J., Holloway, J., Carpenter, J., Goldan, P., Kuster, W., Trainer, M., Montzka, S., McKeen, S., Fehsenfeld, F., 1995. Evaluation of ozone precursor source types using principal component analysis of ambient air measurements in rural Alabama. J. Geophys. Res. Atmos. 100 (D11), 22853–22860. http://dx.doi.org/10.1029/95JD01837.

Cooper, O.R., Eckhardt, S., Crawford, J.H., Brown, C.C., Cohen, R.C., Bertram, T.H., Wooldridge, P., Perring, A., Brune, W.H., Ren, X., Brunner, D., Baughcum, S.L., 2009. Summertime buildup and decay of lightning NO_x and aged thunderstorm outflow above North America. J. Geophys. Res. Atmos. 114 (D1) http://dx.doi.org/10.1029/2008JD010293.

Cooper, O.R., Moody, J.L., Parrish, D.D., Trainer, M., Ryerson, T.B., Holloway, J.S., Hübler, G., Fehsenfeld, F.C., Oltmans, S.J., Evans, M.J., 2001. Trace gas signatures of the airstreams within north Atlantic cyclones: case studies from the north Atlantic regional experiment (NARE '97) aircraft intensive. J. Geophys. Res. 106 (D6), 5437–5456. http://dx.doi.org/10.1029/2000JD900574.

Cooper, O.R., Parrish, D.D., Stohl, A., Trainer, M., Nedelec, P., Thouret, V., Cammas, J.P., Oltmans, S.J., Johnson, B.J., Tarasick, D., Leblanc, T., McDermid, I.S., Jaffe, D., Gao, R., Stith, J., Ryerson, T., Aikin, K., Campos, T., Weinheimer, A., Avery, M.A., 2010. Increasing springtime ozone mixing ratios in the free troposphere over western North America. Nature 463 (7279), 344–348. http://dx.doi.org/10.1038/nature08708.

Dahlmann, K., Grewe, V., Ponater, M., Matthes, S., 2011. Quantifying the contributions of individual NO_x sources to the trend in ozone radiative forcing. Atmos. Environ. 45 (17), 2860–2868.

Dickerson, R.R., 1984. Measurements of reactive nitrogen compounds in the free troposphere. In: CACGP Symposium on Tropospheric Chemistry Part II, vol. 18(12), pp. 2585–2593. http://dx.doi.org/10.1016/0004-6981(84)90323-8.

Drummond, J.W., Volz, A., Ehhalt, D.H., 1985. An optimized chemiluminescence detector for tropospheric NO measurements. J. Atmos. Chem. 2 (3), 287–306.

Duncan, B.N., Logan, J.A., Bey, I., Megretskaia, I.A., Yantosca, R.M., Novelli, P.C., Jones, N.B., Rinsland, C.P., 2007. Global budget of CO, 1988–1997: source estimates and validation with a global model. J. Geophys. Res. 112 (D22), D22301. http://dx.doi.org/10.1029/2007JD008459.

Duncan, B.N., Martin, R.V., Staudt, A.C., Yevich, R., Logan, J.A., 2003. Interannual and seasonal variability of biomass burning emissions constrained by satellite observations. J. Geophys. Res. Atmos. 108 (D2) http://dx.doi.org/10.1029/2002JD002378. ACH 1-1-ACH 1-22.

Dwyer, E., Pinnock, S., Gregoire, J.-M., Pereira, J.M.C., 2000. Global spatial and temporal distribution of vegetation fire as determined from satellite observations. Int. J. Remote Sens. 21 (6–7), 1289–1302. http://dx.doi.org/10.1080/014311600210182.

Ebinghaus, R., Slemr, F., Brenninkmeijer, C.A.M., van Velthoven, P., Zahn, A., Hermann, M., O'Sullivan, D.A., Oram, D.E., 2007. Emissions of gaseous mercury from biomass burning in South America in 2005 observed during CARIBIC flights. Geophys. Res. Lett. 34 (8), L08813.

Eckhardt, S., Stohl, A., Wernli, H., James, P., Forster, C., Spichtinger, N., 2003. A 15 year climatology of warm conveyor belts. J. Clim. 17, 218–237.

Edwards, D.P., Emmons, L.K., Hauglustaine, D.A., Chu, D.A., Gille, J.C., Kaufman, Y.J., Pétron, G., Yurganov, L.N., Giglio, L., Deeter, M.N., Yudin, V., Ziskin, D.C., Warner, J., Lamarque, J.-F., Francis, G.L., Ho, S.P., Mao, D., Chen, J., Grechko, E.I., Drummond, J.R., 2004. Observations of carbon monoxide and aerosols from the Terra satellite: northern hemisphere variability. J. Geophys. Res. Atmos. 109 (D24) http://dx.doi.org/10.1029/2004JD004727.

Ehhalt, D.H., Rohrer, F., Wahner, A., 1992. Sources and distribution of NO_x in the upper troposphere. J. Geophys. Res. 97 (D4), 3725–3738.

Emmons, L.K., Carroll, M.A., Hauglustaine, D.A., Brasseur, G.P., Atherton, C., Penner, J., Sillman, S., Levy II, H., Rohrer, F., Wauben, W.M.F., van Velthoven, P.F.J., Wang, Y., Jacob, D., Bakwin, P., Dickerson, R., Doddridge, B., Gerbig, C., Honrath, R., Hübler, G., Jaffe, D., Kondo, Y., Munger, J.W., Torres, A., Volz-Thomas, A., 1997. Climatologies of NO_x and NO_y: a comparison of data and models. Atmos. Environ. 31 (12), 1851–1904. http://dx.doi.org/10.1016/S1352-2310(96)00334-2.

Eyers, C.J., Addleton, D., Atkinson, K., Broomhead, M.J., Christou, R., Elliff, T., Falk, R., Gee, I., Lee, D.S., Marizy, C., Michot, S., Middel, J., Newton, P., Norman, P., Plohr, M., Raper, D., Stanciou, N., 2005. AERO2K Global Aviation Emissions Inventories for 2002 and 2025. QinetiQ for European Commission under Contract No. G4RD-CT-2000-00382, Farnborough, Hampshire, GU14 0LX.

Fahey, D.W., Eubank, C.S., Hübler, G., Fehsenfeld, F.C., 1985. Evaluation of a catalytic reduction technique for the measurement of total reactive odd-nitrogen NO_y in the atmosphere. J. Atmos. Chem. 3 (4), 435–468.

Feigl, C., Schlager, H., Ziereis, H., Curtius, J., Arnold, F., Schiller, C., 1999. Observation of NO_y uptake by particles in the Arctic tropopause region at low temperatures. Geophys. Res. Lett. 26 (14), 2215–2218. http://dx.doi.org/10.1029/1999GL900338.

Fiedler, V., Nau, R., Ludmann, S., Arnold, F., Schlager, H., Stohl, A., 2009. East Asian SO_2 pollution plume over Europe – part 1: airborne trace gas measurements and source identification by particle dispersion model simulations. Atmos. Chem. Phys. 9 (14), 4717–4728. http://dx.doi.org/10.5194/acp-9-4717-2009.

Fuglestvedt, J.S., Berntsen, T.K., Isaksen, Ivar S.A., Mao, H., Liang, X.-Z., Wang, W.-C., 1999. Climatic forcing of nitrogen oxides through changes in tropospheric ozone and methane; global 3D model studies. Atmos. Environ. 33 (6), 961–977. http://dx.doi.org/10.1016/S1352-2310(98)00217-9.

Gerbig, C., Kley, D., Volz-Thomas, A., Kent, J., Dewey, K., McKenna, D.S., 1996. Fast response resonance fluorescence CO measurements aboard the C-130: instrument characterization and measurements made during north Atlantic regional experiment 1993. J. Geophys. Res. 101 (D22), 29229–29238. http://dx.doi.org/10.1029/95JD03272.

Ghude, S.D., Lal, D.M., Beig, G., van der, A., Ronald, Sable, D., 2010. Rain-induced soil NO_x emission from India during the onset of the summer monsoon: a satellite perspective. J. Geophys. Res. 115 (D16), D16304. http://dx.doi.org/10.1029/2009JD013367.

Gressent, A., Sauvage, B., Defer, E., Pätz, H., Thomas, K., Holle, R., Cammas, J.-P., Nédélec, P., Boulanger, D., Thouret, V., Volz-Thomas, A., 2014. Lightning NO_x influence on large-scale NO_y and O_3 plumes observed over the northern mid-latitudes. Tellus B 66.

Grewe, V., 2007. Impact of climate variability on tropospheric ozone. Sci. Total Environ. 374 (1), 167–181.

Grooss, J.-U., Brühl, C., Peter, T., 1998. Impact of aircraft emissions on tropospheric and stratospheric ozone. Part I: chemistry and 2-D model results. Atmos. Environ. 32 (18), 3173–3184. http://dx.doi.org/10.1016/S1352-2310(98)00016-8.

Hegglin, M.I., Brunner, D., Peter, T., Hoor, P., Fischer, H., Staehelin, J., Krebsbach, M., Schiller, C., Parchatka, U., Weers, U., 2006. Measurements of NO, NO_y, N_2O, and O_3 during SPURT: implications for transport and chemistry in the lowermost stratosphere. Atmos. Chem. Phys. 6 (5), 1331–1350. http://dx.doi.org/10.5194/acp-6-1331-2006.

Holmes, C.D., Tang, Q., Prather, M.J., 2011. Uncertainties in climate assessment for the case of aviation NO. Proc. Natl. Acad. Sci. 108 (27), 10997–11002.

Hoskins, B.J., McIntyre, M.E., Robertson, A.W., 1985. On the use and significance of isentropic potential vorticity maps. Q. J. R. Meteorol. Soc. 111, 877–946.

Huntrieser, H., Feigl, C., Schlager, H., Schröder, F., Gerbig, C., van Velthoven, P., Flatøy, F., Théry, C., Petzold, A., Höller, H., Schumann, U., 2002. Airborne measurements of NO_x, tracer species, and small particles during the European lightning nitrogen oxides experiment. J. Geophys. Res. Atmos. 107 (D11) http://

dx.doi.org/10.1029/2000JD000209. ACH 5-1-ACH 5-24.
Huntrieser, H., Heland, J., Schlager, H., Forster, C., Stohl, A., Aufmhoff, H., Arnold, F., Scheel, H.E., Campana, M., Gilge, S., Eixmann, R., Cooper, O., 2005. Intercontinental air pollution transport from North America to Europe: experimental evidence from airborne measurements and surface observations. J. Geophys. Res. Atmos. 110 (D1) http://dx.doi.org/10.1029/2004JD005045.
Huntrieser, H., Schlager, H., Roiger, A., Lichtenstern, M., Schumann, U., Kurz, C., Brunner, D., Schwierz, C., Richter, A., Stohl, A., 2007. Lightning-produced NO_x over Brazil during TROCCINOX: airborne measurements in tropical and subtropical thunderstorms and the importance of mesoscale convective systems. Atmos. Chem. Phys. 7 (11), 2987–3013. http://dx.doi.org/10.5194/acp-7-2987-2007.
Jaeglé, L., Jacob, D.J., Brune, W.H., Faloona, I.C., Tan, D., Kondo, Y., Sachse, G.W., Anderson, B., Gregory, G.L., Vay, S., Singh, H.B., Blake, D.R., Shetter, R., 1999. Ozone production in the upper troposphere and the influence of aircraft during SONEX: approach of NO_x-saturated conditions. Geophys. Res. Lett. 26 (20), 3081–3084. http://dx.doi.org/10.1029/1999GL900451.
Jaeglé, L., Jacob, D.J., Wang, Y., Weinheimer, A.J., Ridley, B.A., Campos, T.L., Sachse, G.W., Hagen, D.E., 1998. Sources and chemistry of NO_x in the upper troposphere over the United States. Geophys. Res. Lett. 25 (10), 1705–1708.
Jeker, D.P., Pfister, L., Thompson, A.M., Brunner, D., Boccippio, D.J., Pickering, K.E., Wernli, H., Kondo, Y., Staehelin, J., 2000. Measurements of nitrogen oxides at the tropopause: attribution to convection and correlation with lightning. J. Geophys. Res. 105 (D3), 3679–3700. http://dx.doi.org/10.1029/1999JD901053.
Kley, D., McFarland, M., 1980. Chemiluminescence detector for NO and NO_2. Atmos. Technol. 12, 63–69.
Kondo, Y., Morino, Y., Takegawa, N., Koike, M., Kita, K., Miyazaki, Y., Sachse, G.W., Vay, S.A., Avery, M.A., Flocke, F., Weinheimer, A.J., Eisele, F.L., Zondlo, M.A., Weber, R.J., Singh, H.B., Chen, G., Crawford, J., Blake, D.R., Fuelberg, H.E., Clarke, A.D., Talbot, R.W., Sandholm, S.T., Browell, E.V., Streets, D.G., Liley, B., 2004. Impacts of biomass burning in southeast Asia on ozone and reactive nitrogen over the western Pacific in spring. J. Geophys. Res. 109 (D15), D15S12. http://dx.doi.org/10.1029/2003JD004203.
Krishnamurti, T.N., Bhalme, H.N., 1976. Oscillations of a monsoon system. Part I. observational aspects. J. Atmos. Sci. 33 (10), 1937–1954. http://dx.doi.org/10.1175/1520-0469(1976)033<1937:OOAMSP>2.0.CO;2.
Kurtenbach, R., Kleffmann, J., Niedojadlo, A., Wiesen, P., 2012. Primary NO_2 emissions and their impact on air quality in traffic environments in Germany. Environ. Sci. Eur. 24 (1), 1–8. http://dx.doi.org/10.1186/2190-4715-24-21.
Lacis, A.A., Wuebbles, D.J., Logan, J.A., 1990. Radiative forcing of climate by changes in the vertical distribution of ozone. J. Geophys. Res. Atmos. 95 (D7), 9971–9981. http://dx.doi.org/10.1029/JD095iD07p09971.
Lai, S.C., Baker, A.K., Schuck, T.J., van Velthoven, P., Oram, D.E., Zahn, A., Hermann, M., Weigelt, A., Slemr, F., Brenninkmeijer, C.A.M., Ziereis, H., 2010. Pollution events observed during CARIBIC flights in the upper troposphere between South China and the Philippines. Atmos. Chem. Phys. 10 (4), 1649–1660. http://dx.doi.org/10.5194/acp-10-1649-2010.
Lal, D.M., Pawar, S.D., 2009. Relationship between rainfall and lightning over central Indian region in monsoon and premonsoon seasons. Atmos. Res. 92 (4), 402–410. http://dx.doi.org/10.1016/j.atmosres.2008.12.009.
Law, K.S., Stohl, A., Quinn, P.K., Brock, C.A., Burkhart, J.F., Paris, J.-D., Ancellet, G., Singh, H.B., Roiger, A., Schlager, H., Dibb, J., Jacob, D.J., Arnold, S.R., Pelon, J., Thomas, J.L., 2014. Arctic air pollution: new insights from POLARCAT-IPY. Bull. Am. Meteorol. Soc. 95 (12), 1873–1895. http://dx.doi.org/10.1175/BAMS-D-13-00017.1.
Lelieveld, J., Crutzen, P.J., Ramanathan, V., Andreae, M.O., Brenninkmeijer, C.A.M., Campos, T., Cass, G.R., Dickerson, R.R., Fischer, H., de Gouw, J.A., Hansel, A., Jefferson, A., Kley, D., de Laat, A.T.J., Lal, S., Lawrence, M.G., Lobert, J.M., Mayol-Bracero, O.L., Mitra, A.P., Novakov, T., Oltmans, S.J., Prather, K.A., Reiner, T., Rodhe, H., Scheeren, H.A., Sikka, D., Williams, J., 2001. The Indian ocean experiment: widespread air pollution from south and southeast Asia. Science 291 (5506), 1031–1036. http://dx.doi.org/10.1126/science.1057103.
Li, Q., Jacob, D.J., Yantosca, R.M., Heald, C.L., Singh, H.B., Koike, M., Zhao, Y., Sachse, G.W., Streets, D.G., 2003. A global three-dimensional model analysis of the atmospheric budgets of HCN and CH3CN: constraints from aircraft and ground measurements. J. Geophys. Res. 108 (D21).
Liang, Q., Rodriguez, J.M., Douglass, A.R., Crawford, J.H., Olson, J.R., Apel, E., Bian, H., Blake, D.R., Brune, W., Chin, M., Colarco, P.R., da Silva, A., Diskin, G.S., Duncan, B.N., Huey, L.G., Knapp, D.J., Montzka, D.D., Nielsen, J.E., Pawson, S., Riemer, D.D., Weinheimer, A.J., Wisthaler, A., 2011. Reactive nitrogen, ozone and ozone production in the Arctic troposphere and the impact of stratosphere-troposphere exchange. Atmos. Chem. Phys. 11 (24), 13181–13199. http://dx.doi.org/10.5194/acp-11-13181-2011.
Liousse, C., Guillaume, B., Grégoire, J.M., Mallet, M., Galy, C., Pont, V., Akpo, A., Bedou, M., Castéra, P., Dungall, L., Gardrat, E., Granier, C., Konaré, A., Malavelle, F., Mariscal, A., Mieville, A., Rosset, R., Serça, D., Solmon, F., Tummon, F., Assamoi, E., Yoboué, V., van Velthoven, P., 2010. Updated African biomass burning emission inventories in the framework of the AMMA-IDAF program, with an evaluation of combustion aerosols. Atmos. Chem. Phys. 10 (19), 9631–9646. http://dx.doi.org/10.5194/acp-10-9631-2010.
Liu, S.C., Kley, D., Mcfarland, M., Mahlman, J.D., Levy, H., 1980. On the origin of tropospheric ozone. J. Geophys. Res. Ocean. Atmos. 85 (Nc12), 7546–7552.
Madronich, S., Flocke, S., Zeng, J., Petropavlovskikh, I., Lee-Taylor, J., 2002. Tropospheric Ultraviolet-visible Model (TUV) Version 4.1. P.O. Box 3000, Boulder, Colorado 80307.
McCormack, J.P., Hood, L.L., 1997. The frequency and size of ozone 'qmini-hole'q events at northern midlatitudes in February. Geophys. Res. Lett. 24 (21), 2647–2650. http://dx.doi.org/10.1029/97GL02642.
Miyazaki, K., Eskes, H.J., Sudo, K., Zhang, C., 2014. Global lightning NO_x production estimated by an assimilation of multiple satellite data sets. Atmos. Chem. Phys. 14 (7), 3277–3305. http://dx.doi.org/10.5194/acp-14-3277-2014.
Miyazaki, Y., Kondo, Y., Koike, M., Fuelberg, H.E., Kiley, C.M., Kita, K., Takegawa, N., Sachse, G.W., Flocke, F., Weinheimer, A.J., Singh, H.B., Eisele, F.L., Zondlo, M., Talbot, R.W., Sandholm, S.T., Avery, M.A., Blake, D.R., 2003. Synoptic-scale transport of reactive nitrogen over the western Pacific in spring. J. Geophys. Res. 108 (D20), 8788.
Neuman, J.A., Huey, L.G., Ryerson, T.B., Fahey, D.W., 1999. Study of inlet materials for sampling atmospheric nitric acid. Environ. Sci. Technol. 33 (7), 1133–1136.
Orville, R.E., Huffines, G.R., Burrows, W.R., Holle, R.L., Cummins, K.L., 2002. The North American lightning detection network (NALDN) – first results: 1998-2000. Mon. Weather Rev. 130 (8), 2098–2109. http://dx.doi.org/10.1175/15200493(2002)130<2098:TNALDN>2.0.CO;2.
Pandey Deolal, S., Brunner, D., Steinbacher, M., Weers, U., Staehelin, J., 2012. Long-term in situ measurements of NO_x and NO_y at Jungfraujoch 1998-2009: time series analysis and evaluation. Atmos. Chem. Phys. 12 (5), 2551–2566. http://dx.doi.org/10.5194/acp-12-2551-2012.
Parrish, D.D., Trainer, M., Buhr, M.P., Watkins, B.A., Fehsenfeld, F.C., 1991. Carbon monoxide concentrations and their relation to concentrations of total reactive oxidized nitrogen at two rural U.S. sites. J. Geophys. Res. Atmos. 96 (D5), 9309–9320. http://dx.doi.org/10.1029/91JD00047.
Pétron, G., Granier, C., Khattatov, B., Yudin, V., Lamarque, J.-F., Emmons, L., Gille, J., Edwards, D.P., 2004. Monthly CO surface sources inventory based on the 2000-2001 MOPITT satellite data. Geophys. Res. Lett. 31 (21) http://dx.doi.org/10.1029/2004GL020560.
Rauthe-Schöch, A., Baker, A.K., Schuck, T.J., Brenninkmeijer, C.A.M., Zahn, A., Hermann, M., Stratmann, G., Ziereis, H., van Velthoven, P.F.J., Lelieveld, J., 2015. Trapping, chemistry and export of trace gases in the South Asian summer monsoon observed during CARIBIC flights in 2008. Atmos. Chem. Phys. Discuss. 15 (5), 6967–7018. http://dx.doi.org/10.5194/acpd-15-6967-2015.
Richter, A., Burrows, J.P., 2002. Tropospheric NO_2 from GOME measurements. Adv. Space Res. 29 (11), 1673–1683.
Richter, A., Burrows, J.P., Nusz, H., Granier, C., Niemeier, U., 2005. Increase in tropospheric nitrogen dioxide over China observed from space. Nature 437 (7055), 129–132. http://dx.doi.org/10.1038/nature04092.
Ridley, B., Ott, L., Pickering, K., Emmons, L., Montzka, D., Weinheimer, A., Knapp, D., Grahek, F., Li, L., Heymsfield, G., McGill, M., Kucera, P., Mahoney, M.J., Baumgardner, D., Schultz, M., Brasseur, G., 2004. Florida thunderstorms: a faucet of reactive nitrogen to the upper troposphere. J. Geophys. Res. Atmos. 109 (D17) http://dx.doi.org/10.1029/2004JD004769.
Ridley, B.A., Howlett, L.C., 1974. An instrument for nitric oxide measurements in the stratosphere. Rev. Sci. Instrum. 45 (6), 742–746. http://dx.doi.org/10.1063/1.1686726.
Roberts, G., Wooster, M.J., Lagoudakis, E., 2009. Annual and diurnal african biomass burning temporal dynamics. Biogeosciences 6 (5), 849–866. http://dx.doi.org/10.5194/bg-6-849-2009.
Roiger, A., Schlager, H., Schäfler, A., Huntrieser, H., Scheibe, M., Aufmhoff, H., Cooper, O.R., Sodemann, H., Stohl, A., Burkhart, J., Lazzara, M., Schiller, C., Law, K.S., Arnold, F., 2011. In-situ observation of Asian pollution transported into the Arctic lowermost stratosphere. Atmos. Chem. Phys. 11 (21), 10975–10994. http://dx.doi.org/10.5194/acp-11-10975-2011.
Rotty, R.M., 1987. Estimates of seasonal variation in fossil fuel CO_2 emissions. Tellus B 39B (1–2), 184–202. http://dx.doi.org/10.1111/j.1600-0889.1987.tb00281.x.
Russell, A.R., Valin, L.C., Cohen, R.C., 2012. Trends in OMI NO_2 observations over the United States: effects of emission control technology and the economic recession. Atmos. Chem. Phys. 12 (24), 12197–12209. http://dx.doi.org/10.5194/acp-12-12197-2012.
Scharffe, D., Slemr, F., Brenninkmeijer, C.A.M., Zahn, A., 2012. Carbon monoxide measurements onboard the CARIBIC passenger aircraft using UV resonance fluorescence. Atmos. Meas. Tech. 5 (7), 1753–1760. http://dx.doi.org/10.5194/amt-5-1753-2012.
Scheele, M.P., Siegmund, P.C., van Velthoven, P.F.J., 1996. Sensitivity of trajectories to data resolution and its dependence on the starting point: in or outside a tropopause fold. Meteorol. Appl. 3 (3), 267–273. http://dx.doi.org/10.1002/met.5060030308.
Schlager, H., Konopka, P., Schulte, P., Schumann, U., Ziereis, H., Arnold, F., Klemm, M., Hagen, D.E., Whitefield, P.D., Ovarlez, J., 1997. In situ observations of air traffic emission signatures in the North Atlantic flight corridor. J. Geophys. Res. Atmos. 102 (D9), 10739–10750. http://dx.doi.org/10.1029/96JD03748.
Schuck, T.J., Brenninkmeijer, C.A.M., Baker, A.K., Slemr, F., von Velthoven, P.F.J., Zahn, A., 2010. Greenhouse gas relationships in the Indian summer monsoon plume measured by the CARIBIC passenger aircraft. Atmos. Chem. Phys. 10 (8), 3965–3984. http://dx.doi.org/10.5194/acp-10-3965-2010.
Schulte, P., Schlager, H., 1996. In-flight measurements of cruise altitude nitric oxide emission indices of commercial jet aircraft. Geophys. Res. Lett. 23 (2), 165–168. http://dx.doi.org/10.1029/95GL03691.
Schumann, U., Huntrieser, H., 2007. The global lightning-induced nitrogen oxides source. Atmos. Chem. Phys. 7 (14), 3823–3907. http://dx.doi.org/10.5194/acp-7-3823-2007.
Singh, H.B., Anderson, B.E., Brune, W.H., Cai, C., Cohen, R.C., Crawford, J.H., Cubison, M.J., Czech, E.P., Emmons, L., Fuelberg, H.E., Huey, G., Jacob, D.J.,

Jimenez, J.L., Kaduwela, A., Kondo, Y., Mao, J., Olson, J.R., Sachse, G.W., Vay, S.A., Weinheimer, A., Wennberg, P.O., Wisthaler, A., 2010. Pollution influences on atmospheric composition and chemistry at high northern latitudes: boreal and California forest fire emissions. Atmos. Environ. 44 (36), 4553–4564. http://dx.doi.org/10.1016/j.atmosenv.2010.08.026.

Singh, H.B., Salas, L., Herlth, D., Kolyer, R., Czech, E., Avery, M., Crawford, J.H., Pierce, R.B., Sachse, G.W., Blake, D.R., Cohen, R.C., Bertram, T.H., Perring, A., Wooldridge, P.J., Dibb, J., Huey, G., Hudman, R.C., Turquety, S., Emmons, L.K., Flocke, F., Tang, Y., Carmichael, G.R., Horowitz, L.W., 2007. Reactive nitrogen distribution and partitioning in the North American troposphere and lowermost stratosphere. J. Geophys. Res. Atmos. 112 (D12) http://dx.doi.org/10.1029/2006JD007664.

Singh, H.B., Thompson, A.M., Schlager, H., 1999. SONEX airborne mission and coordinated POLINAT-2 activity: overview and accomplishments. Geophys. Res. Lett. 26 (20), 3053–3056. http://dx.doi.org/10.1029/1999GL900588.

Slemr, F., Ebinghaus, R., Brenninkmeijer, C.A.M., Hermann, M., Kock, H.H., Martinsson, B.G., Schuck, T., Sprung, D., van Velthoven, P., Zahn, A., Ziereis, H., 2009. Gaseous mercury distribution in the upper troposphere and lower stratosphere observed onboard the CARIBIC passenger aircraft. Atmos. Chem. Phys. 9 (6), 1957–1969. http://dx.doi.org/10.5194/acp-9-1957-2009.

Stevenson, D.S., Young, P.J., Naik, V., Lamarque, J.-F., Shindell, D.T., Voulgarakis, A., Skeie, R.B., Dalsoren, S.B., Myhre, G., Berntsen, T.K., Folberth, G.A., Rumbold, S.T., Collins, W.J., MacKenzie, I.A., Doherty, R.M., Zeng, G., van Noije, T.P.C., Strunk, A., Bergmann, D., Cameron-Smith, P., Plummer, D.A., Strode, S.A., Horowitz, L., Lee, Y.H., Szopa, S., Sudo, K., Nagashima, T., Josse, B., Cionni, I., Righi, M., Eyring, V., Conley, A., Bowman, K.W., Wild, O., Archibald, A., 2013. Tropospheric ozone changes, radiative forcing and attribution to emissions in the atmospheric chemistry and climate model intercomparison project (ACCMIP). Atmos. Chem. Phys. 13 (6), 3063–3085. http://dx.doi.org/10.5194/acp-13-3063-2013.

Stohl, A., Trainer, M., Ryerson, T.B., Holloway, J.S., Parrish, D.D., 2002. Export of NO_y from the North American boundary layer during 1996 and 1997 north Atlantic regional experiments. J. Geophys. Res. 107 (D11), 4131.

Talbot, R.W., Dibb, J.E., Klemm, K.I., Bradshaw, J.D., Sandholm, S.T., Blake, D.R., Sachse, G.W., Collins, J., Heikes, B.G., Gregory, G.L., Anderson, B.E., Singh, H.B., Thornton, D.C., Merrill, J.T., 1996. Chemical characteristics of continental outflow from Asia to the troposphere over the western Pacific Ocean during september–october 1991: results from PEM-west A. J. Geophys. Res. 101 (D1), 1713–1725. http://dx.doi.org/10.1029/95JD01044.

Talbot, R.W., Dibb, J.E., Scheuer, E.M., Kondo, Y., Koike, M., Singh, H.B., Salas, L.B., Fukui, Y., Ballenthin, J.O., Meads, R.F., Miller, T.M., Hunton, D.E., Viggiano, A.A., Blake, D.R., Blake, N.J., Atlas, E., Flocke, F., Jacob, D.J., Jaegle, L., 1999. Reactive nitrogen budget during the NASA SONEX mission. Geophys. Res. Lett. 26 (20), 3057–3060. http://dx.doi.org/10.1029/1999GL900589.

Talukdar, R.K., Burkholder, J.B., Schmoltner, A.-M., Roberts, J.M., Wilson, R.R., Ravishankara, A.R., 1995. Investigation of the loss processes for peroxyacetyl nitrate in the atmosphere: UV photolysis and reaction with OH. J. Geophys. Res. 100 (D7), 14163–14173. http://dx.doi.org/10.1029/95JD00545.

Thomas, K., Berg, M., Boulanger, D., Houben, N., Nedelec, P., Gressent, A., Pätz, H.W., Thouret, V., Volz-Thomas, A., 2015. Climatology of NOy in the troposphere and UT/LS from measurements made in MOZAIC. Tellus B 67, 28793. http://dx.doi.org/10.3402/tellusb.v67.28793.

Thompson, A.M., Sparling, L.C., Kondo, Y., Anderson, B.E., Gregory, G.L., Sachse, G.W., 1999. Perspectives on NO, NO_y, and fine aerosol sources and variability during SONEX. Geophys. Res. Lett. 26 (20), 3073–3076. http://dx.doi.org/10.1029/1999GL900581.

Voigt, C., Schumann, U., Jurkat, T., Schäuble, D., Schlager, H., Petzold, A., Gayet, J.-F., Krämer, M., Schneider, J., Borrmann, S., Schmale, J., Jessberger, P., Hamburger, T., Lichtenstern, M., Scheibe, M., Gourbeyre, C., Meyer, J., Kübbeler, M., Frey, W., Kalesse, H., Butler, T., Lawrence, M.G., Holzäpfel, F., Arnold, F., Wendisch, M., Döpelheuer, A., Gottschaldt, K., Baumann, R., Zöger, M., Sölch, I., Rautenhaus, M., Dörnbrack, A., 2010. In-situ observations of young contrails – overview and selected results from the CONCERT campaign. Atmos. Chem. Phys. 10 (18), 9039–9056. http://dx.doi.org/10.5194/acp-10-9039-2010.

Volz-Thomas, A., Berg, M., Heil, T., Houben, N., Lerner, A., Petrick, W., Raak, D., Pätz, H.-W., 2005. Measurements of total odd nitrogen (NO_y) aboard MOZAIC in-service aircraft: instrument design, operation and performance. Atmos. Chem. Phys. 5 (3), 583–595. http://dx.doi.org/10.5194/acp-5-583-2005.

Wang, Y., Liu, S.C., Anderson, B.E., Kondo, Y., Gregory, G.L., Sachse, G.W., Vay, S.A., Blake, D.R., Singh, H.B., Thompson, A.M., 2000. Evidence of convection as a major source of condensation nuclei in the northern midlatitude upper troposphere. Geophys. Res. Lett. 27 (3), 369–372. http://dx.doi.org/10.1029/1999GL010930.

Zahn, A., Brenninkmeijer, C.A.M., Asman, W.A.H., Crutzen, P.J., Heinrich, G., Fischer, H., Cuijpers, J.W.M., van Velthoven, P.F.J., 2002. Budgets of O_3 and CO in the upper troposphere: CARIBIC passenger aircraft results 1997-2001. J. Geophys. Res. 107 (D17), 4337.

Zahn, A., Weppner, J., Widmann, H., Schlote-Holubek, K., Burger, B., Kühner, T., Franke, H., 2012. A fast and precise chemiluminescence ozone detector for eddy flux and airborne application. Atmos. Meas. Tech. 5 (2), 363–375. http://dx.doi.org/10.5194/amt-5-363-2012.

Zhang, Q., Streets, D.G., He, K., Wang, Y., Richter, A., Burrows, J.P., Uno, I., Jang, C.J., Chen, D., Yao, Z., Lei, Y., 2007. NO_x emission trends for China, 1995–2004: the view from the ground and the view from space. J. Geophys. Res. 112 (D22), D22306. http://dx.doi.org/10.1029/2007JD008684.

Ziereis, H., Minikin, A., Schlager, H., Gayet, J.F., Auriol, F., Stock, P., Baehr, J., Petzold, A., Schumann, U., Weinheimer, A., Ridley, B., Ström, J., 2004. Uptake of reactive nitrogen on cirrus cloud particles during INCA. Geophys. Res. Lett. 31 (5), L05115. http://dx.doi.org/10.1029/2003GL018794.

Ziereis, H., Schlager, H., Schulte, P., van Velthoven, P.F.J., Slemr, F., 2000. Distributions of NO, NOx, and NOy in the upper troposphere and lower stratosphere between 28° and 61°N during POLINAT 2. J. Geophys. Res. 105 (D3), 3653–3664.

Zipser, E.J., Liu, C., Cecil, D.J., Nesbitt, S.W., Yorty, D.P., 2006. Where are the most intense thunderstorms on Earth? Bull. Am. Meteorol. Soc. 87 (8), 1057–1071. http://dx.doi.org/10.1175/BAMS-87-8-1057.